Genomic and phenotypic evolution of nematode-infecting microsporidia

Lina Wadi[1], Hala Tamim El Jarkass[1*], Tuan D. Tran[2*], Nizar Islah[1], Robert J. Luallen[2], and Aaron W. Reinke[1#]
[1] Department of Molecular Genetics, University of Toronto, Toronto, ON, Canada
[2] Department of Biology, San Diego State University, San Diego, CA 92182, USA
#Corresponding author
*These authors contributed equally

aaron.reinke@utoronto.ca

Abstract
Microsporidia are a large phylum of intracellular parasites that can infect most types of animals. Species in the *Nematocida* genus can infect nematodes including *Caenorhabditis elegans*, which has become an important model to study mechanisms of microsporidia infection. To understand the genomic properties and evolution of nematode-infecting microsporidia, we sequenced the genomes of nine species of microsporidia, including two genera, *Enteropsectra* and *Pancytospora,* without any previously sequenced genomes. Phylogenetic analysis shows that *Nematocida* is composed of two groups of species. Core cellular processes, including metabolic pathways, are mostly conserved across genera of nematode-infecting microsporidia. Each species encodes unique proteins belonging to large gene families that are likely used to interact with host cells. Most strikingly, we observed one such family, NemLGF1, is present in both *Nematocida* and *Pancytospora* species, suggesting horizontal gene transfer between species from different genera. To understand how *Nematocida* phenotypic traits evolved, we measured the host range, tissue specificity, spore size, and polar tube length of several species in the genus. Our results demonstrate that the ability to infect multiple tissues was likely recently lost in *N. homosporus* and that species with longer polar tubes are able to infect multiple tissues. Together, our work details both genomic and trait evolution between related microsporidia species and provides a useful resource for further understanding microsporidia evolution and infection mechanisms.

Introduction

Microsporidia are a large phylum of obligate intracellular parasites[1]. They were the first eukaryotic parasite to have a genome sequenced which revealed the smallest known eukaryotic genome[2]. In the last 20 years, genomes from ~35 species have been sequenced, with the smallest genomes belonging to *Encephalitozoon* spp. encoding only ~1800 proteins[3]. Analysis of their genomes has shown that microsporidia are either the earliest diverging group of fungi or a sister group to fungi[4–6]. The evolution of microsporidia coincided with the loss of flagellum and the gain of a novel infection apparatus known as the polar tube[3]. Early-diverging microsporidian species retained a mitochondrial genome, but underwent moderate genomic loss[7,8]. Consistent with their evolution as obligate intracellular parasites, however, canonical microsporidia have undergone extensive genomic reduction, which has resulted in the loss of the mitochondrial genome and many other metabolic and regulatory proteins[9]. Additionally, microsporidian ribosomes have lost both proteins and ribosomal RNA expansion segments, resulting in the smallest known eukaryotic ribosomes[10]. Microsporidian proteins are also reduced, being on average ~15% shorter than their fungal orthlogs[2,11]. While these larger phylogenetic changes are well studied, it is less clear how individual microsporidia genera have evolved. One interesting example is the *Enterocytozoon* genus, which has undergone a linage-specific loss of many genes involved in glycolysis[12].

Microsporidia have evolved to infect a wide range of different hosts. Over 1400 microsporidian species have been characterized and about half of all animal phyla as well as some protists are reported to be infected[13]. Most individual microsporidian species only infect one or two closely related hosts, but ~2% have been reported to infect more than five species. The genomic differences that account for some microsporidia having a broader host range, consistent with being a generalist, is mostly unknown but a comparison between a pair of mosquito-infecting species showed that the generalist contains a much smaller genome than the specialiast[11]. Once inside a host, most microsporidia only infect a single tissue, but ~11% can infect four or more tissues. The mechanisms that restrict microsporidia infection to specific tissues are largely unknown, but longer polar tubes correlate with infecting tissues other than the intestine, suggesting that the longer tube is needed to access these other tissues[13,14]. Interestingly, microsporidia that infect multiple host species are more likely to infect more tissues, suggesting that the selective pressures for these traits may be related[13]. Microsporidia display great diversity in their morphological and infection properties, even within related clades, suggesting these parasites may be particularly plastic in their ability to evolve phenotypic traits[13].

Several species of microsporidia have been found to infect free-living nematodes[14–17]. The first of these to be characterized was *Nematocida parisii,* which naturally infects the model organism *Caenorhabditis elegans*[16]. This microsporidian species has been used as model to understand microsporidian infection of a host, host immune responses to infection, and identify inhibitors of microsporidia infection[17–23]. Additional species that infect the intestine, *N. ausubeli*, and *N. ironsii,* have also been identified[16,17]. More recently, another species, *N. displodere,* was found which infects other tissues of *C. elegans,* including the neurons, muscle, and epidermis[14]. Several other species infecting both *C. elegans* and other free-living nematodes have also been identified[15]. Besides *Nematocida*, two other genera, *Enteropsectra* and *Pancytospora,* have been reported to infect nematodes and shown to be more closely related to species of microsporidia that infect humans[15].

Four species of nematode-infecting microsporidia from the *Nematocida* genus, have been sequenced, revealing moderate-sized genomes encoding between ~2300-2800 proteins. Many of the proteins in these genomes were found to have the potential to directly interact with their hosts, including many proteins that belong to large gene families[5,14,17]. One such large gene family, NemLGF1, contains a signal for secretion and between ~160-240 proteins have been identified in each of the *N. parisii*, *N. ironsii*, and *N. ausubeli* genomes, including many linage specific expansions[17]. Another family, NemLGF2, is present in only *N. displodere* and contains over 230 proteins, about half of which contain a RING domain, which is thought to involved in protein-protein interactions[15].

Here we present a comprehensive and comparative analyses of multiple genomes of nematode-infecting microsporidia. To elucidate the genomic properties of nematode-infecting microsporidia and to understand evolution within *Nematocida*, we sequenced nine additional microsporidian species, including three newly identified species. By analyzing 13 nematode-infecting microsporidian species, we show that *Nematocida* forms two groups and that *Enteropsectra* and *Pancytospora* form a sister group to the marine invertebrate- and human-infecting *Enterocytozoon*. We find most conserved cellular processes are retained in *Nematocida* and that the metabolic capacity is largely similar between the genera of nematode-infecting microsporidia. We identified many novel large gene families including, surprisingly, members of NemLGF1 in *Pancytospora* species. Finally, we characterized the phenotypic properties of *Nematocida* species and describe the gain and loss of these traits throughout evolution. Our study reveals evolutionary mechanisms of nematode-infecting microsporidia and provides a valuable resource for the use of nematodes to study mechanisms of microsporidian infection.

Results

Sequencing, assembling, and phylogenetic analysis of microsporidia genomes

Previous efforts in discovering microsporidia in free-living terrestrial nematodes has revealed a diversity of species, but so far only four species from a single genus have been sequenced[5,14,15,17]. To further understand the genomic diversity of nematode-infecting microsporidia, we sequenced nine additional species, including two genera that had not been previously sequenced. Six of these microsporidian species have been previously reported[15]. Three of them we recently discovered through sampling of wild nematode populations; *Nematocida ferruginous* from France, *Nematocida cider* from the United States, and *Nematocida botruosus* from Canada. To sequence these genomes, we removed contaminating bacteria from microsporidia-infected nematodes using antibiotics, cultured infections in the host animals, isolated spores, and extracted DNA. We sequenced a single isolate for each species, except for *N. ferruginous* for which we sequenced three strains that have high similarity to one another (Fig. S1). Information on each microsporidia species, host, and isolation location is presented in Table S1. Microsporidian genomes were assembled and contaminating DNA removed (See Methods and Table S2). Proteins from each genome were predicted and annotated (Table S3). These new microsporidian genome assemblies were assessed on the basis of contig continuity and protein conservation and were demonstrated to be of high quality relative to previously assembled microsporidian genomes (Fig. 1D, E, and Table S4).

To determine the relative relationships between microsporidia species we performed phylogenetic analysis. Using OrthoFinder[24], we generated a phylogenetic tree of our nine newly assembled microsporidia species, 35 previously sequenced microsporidia genomes, and the outgroup *Rozella allomycis* (Fig. 1A and Table S5). This tree shows that *Nematocida* genomes form two groups. The first identified *Nematocida* species, *N. parisii*, forms a group with *N. ausubeli*, *N. ironsii*, *N. major*, and *N. minor*; we refer to these species as the "*Parisii* group"[15–17]. The second group contains the more recently identified *N. displodere* along with *N. homosporus*, *N. cider*, *N. ferruginous,* and *N. botruosus;* we refer to these species as the "*Displodere* group"[14,15]. The relative positions of the *Nematocida* species are highly supported by several phylogenetic trees (Fig. 1A and Fig. S2). As was described previously from 18s rDNA and β–tubulin sequences, the species *Enteropsectra breve*, *Pancytospora philotis*, and *Pancytospora epiphaga* belong to the large cluster of microsporidia species referred to as the Enterocytozoonida clade [13,15,25,26]. Our whole genome based tree replicates this previously described phylogeny and demonstrates that these three non-*Nematocida* species are most closely related to the human-infecting *Vittaforma corneae*, and together they form a sister group to the *Enterocytozoon*[12,27].

Conservation and divergence of proteins in microsporidia genomes

Microsporidia have the smallest known eukaryotic genomes, but genome size and protein content can vary greatly between species[3]. In *Nematocida,* we see consistently small genome sizes that range from ~3.1 to 4.7 megabases. The two *Pancytospora* species are similar to each other, with genome sizes of 4.2 and 4.6 megabases. In contrast, the ~6.0 megabase *E. breve* is the largest of our nematode-infecting microsporidia species genomes (Fig. 1C). We see similar trends in predicted number of proteins, with *N. botruosus* having the fewest proteins (2159) and *E. breve* having the most predicted proteins (3531) (Fig. 1B). Although microsporidia species can have large amounts of non-coding DNA that make their genomes much larger relative to their protein content[11], among nematode-infecting microsporidia, we observe a strong correlation between protein content and genome size (Fig. S3).

Microsporidia are known to have lost many conserved eukaryotic proteins, including those involved in metabolism[9]. To determine the conservation of metabolic function in nematode-infecting microsporidia species, we analyzed proteins encoded by microsporidia genomes using GO term categories. We first determined the number of proteins from each microsporidia species that belong to a set of GO terms that cover most conserved eukaryotic cellular processes (Fig. 2). This analysis reveled that many cellular processes were either lost or greatly reduced in the canonical microsporidia, which has been previously observed[7]. We then determined the proteins from each microsporidian species that belonged to eight metabolic categories (Fig. S4-11, summarized in Fig. 3). As has been previously observed, we see that the *Enterocytozoon* contains many losses in metabolic pathways, and in particular those involved in energy production[12]. As the genera *Pancytospora* and *Enteropsectra,* along with *V. cornea,* form a sister group to the *Enterocytozoon,* we sought to determine how the metabolic capacity of these groups of species compared. We observe that *Pancytospora* and *Enteropsectra* have a similar metabolic capacity compared to most other microsporidia species, including the *Nematocida* (Fig. 3). However, there are several notable differences between the genera, with *Pancytospora* and *Enteropsectra* having losses in glutathione biosynthesis and the *Nematocida* having losses in phosphatidylinositol biosynthesis.

Both RNAi and mRNA splicing pathways have been lost multiple times from microsporidia genomes[11,28]. *Nematocida* was previously observed to not include either of these pathways[3]. We searched through the genomes of *Pancytospora* and *Enteropsectra* and found that splicing pathways were missing in these genomes, as in their closest sequenced relative *V. cornea*[3]. However, the three genomes from *Pancytospora* and *Enteropsectra* each encode RNAi pathway proteins (Table S6).

Nematode-infecting microsporidia contain many large, expanded gene families

A striking feature of microsporidia genomes are abundant large gene families that contain paralogous family members with either signal peptide or transmembrane domains[9,17]. Using a previously described bioinformatic approach[17], we analyzed the large gene family content of nematode-infecting microsporidia, identifying 39 families in 13 species (Fig. 4 and Table S7). We observed that every species had at least one large gene family, with six species having at least five families with more than 10 members each. Some of these families have many members, with 5 families (NemLGF1, NemLGF2, NemLGF11, PanLGF1, and EbrLGF1) containing more than 100 members in at least one species. Previously, we had observed that almost all large gene families are specific to individual clades of microsporidia species[17]. Most families (31/39) in nematode-infecting microsporidia have at least 10 members in only one species. The families we identified in *Pancytospora* and *Enteropsectra* are also unique to these species and not found in *V. cornea*. Some of the large gene families, such NemLGF11, are present in small numbers in other species, but are only greatly expanded in one of the species. To determine if any of the large gene families identified in nematode-infecting microsporidia were present in other microsporidian species, we searched other microsporidia genomes using family-specific models (Table S8). The only family with more than 10 members present in another species is NemLGF27, which contains the previously described InterB family containing the Pfam domain Duf1609, which is present in NemLGF27 family members[29].

One of the most abundant *Nematocida* large gene families is NemLGF1[5,17]. This large family was previously found in the genomes of *N. parisii*, *N. ausubeli*, and *N. ironsii*, with each species containing between 160-240 proteins[17]. We also observe 105 members of this this family in *N. major*. We do not observe this family in *N. minor* or any of the genomes in the *Displodere* group, suggesting that the family appeared in the *Parisii* group after the divergence of *N. minor*. Strikingly,

we find that the NemLGF1 family is also present in *P. philotis* (81 members) and *P. epiphaga* (45 members). We generated a phylogenetic tree using all the members from these six species, which shows distinct expansions of NemLGF1 proteins in the *Nematocida* and *Pancytospora* species (Fig. 5A). Using minimal ancestor deviation to root this tree, we find poor support for the root of the tree, suggesting our data is consistent with either group being the origin[30] (Fig. S12). To determine the similarity of NemLGF1 protein from *Nematocida* and *Pancytospora* species, we used AlphaFold to model the protein structures (Fig. 5B and C)[31,32]. We find that NemLGF1 proteins consist of three main domains (N-terminal, middle, and C-terminal). The N-terminal and middle domains are similar (RSDM of 1.6 Å for N-terminal domain and 1.2 Å for middle domain) between *N. parisii* member NEPG_02057 and *P. epiphaga* member PAEPH01_0103 (Fig. 5D and E). However, the C-terminal domains form a bundle of alpha helices that are less conserved (RSDM of 18.3 Å) (Fig. 5F). We also compared an *N. ausubeli* NemLGF1 member NERG_01890 to *N. parisii* NEPG_02057, and observed similar trends, although the C-terminal domains were more conserved (RSDM 4.5 Å) than with *P. epiphaga* PAEPH01_0103 (Fig. S13A-E).

To begin to understand the biochemical function of these nematode infecting large gene families, we generated structural models for the four other largest families using Alphafold (Fig. S13F-I). None of these families have apparent structural similarity to other solved proteins, with the exception of NemLGF2, which shares similarity to Leucine Rich Repeat proteins (Fig. S13I). This family was previously described in *N. displodere* and we also observe large expansions of this family in *N. ferruginous* and *N. homosporous,* but not in *N. cider*. As previously shown, although we detect a member of this family in the *Parisii* group species, we only observe expansions of this family within some *Displodere* group species.

Evolution of *Nematocida* phenotypic traits

Microsporidia often only infect one or more closely related host species, but generalists that infect many hosts have also been observed[33]. Previous work in *Nematocida* have described species with more restricted host specificity, such as *N. parisii* and *N. ausubeli,* as well as those with a broader host range, like *N. displodere* and *N. homosporus*[15,34]*.* To characterize the host range of the novel species we isolated, we set up experimental infections against seven different nematode hosts. As controls, we also challenged each of these hosts with *N. parisii* and *N. ausubeli*. After 4 days of infection, we fixed and stained populations of animals using direct yellow 96[18] and quantified the proportion of the population that produced microsporidia spores (Fig. 6A). For *N. parisii* and *N. ausubeli*, we observed strong infection of *C. elegans* and *C. briggsae*, which had been reported previously[15]. *N. ausubeli* also infected a modest percent of *C. tropicalis* and a small percent of *C. nigoni*, while *N. parisii* infected a small percent of *C. tropicalis*. These two species could not infect any of the other hosts. These results are consistent with what has been previously reported[15]. For *N. botruosus*, we only observed infection of its native host, and none of the other six host species tested. In contrast, *N. cider* could infect all hosts tested to some extent (Fig. 6B) with *C. elegans* being the most infected at 85.6% and *Panagrellus.* sp. 2 being the least infected at 7.4%. For *N. ferruginous*, we were unable to observe more than 50% of animal infected for any nematode species, even when using a high concentration of spores. However, even at this level of infection, we observed infection of *C. elegans, C. briggsae,* and *C. tropicalis.* Additionally, we saw infection in *C. remanei* and *Oscheius tipulae*, which were species that none of the other microsporidia besides *N. cider* could infect (Fig. S14). Our data suggests that *N. botruosus* has a specialized host range, whereas *N. cider* and *N. ferruginous* appear to be generalists.

Microsporidia mostly infect only one tissue, but some microsporidia, including *N. displodere*, have been shown to infect multiple tissues[13]. During our infection experiments, we only ever observed

spore formation in the intestine for *N. botruosus* but observed infection in other tissues for *N. cider* and *N. ferruginous* (Fig. S15A-C). Additionally, during prolonged infection with *N. cider* or *N. ferruginous*, the entire animal turns brown, suggesting that infection is occurring throughout the animal (Fig. S15D-E). To further characterize which tissues *N. cider* and *N. ferruginous* infect, we used *C. elegans* strains with GFP specifically expressed in either the intestine, epidermis, or body wall muscle (Fig. 6C). We observed *N. ferruginous* could infect both the muscle and the epidermis but we did not see productive infection in the intestine. In contrast, *N. cider* infection was seen in all three tissues, the muscle, epidermis, and intestine, although at a lower frequency in the intestine (Fig. 6D).

We recently showed that the *C. elegans* protein AAIM-1 is necessary for efficient invasion by *N. parisii*[19]. This protein is secreted and likely functions in the intestinal lumen. Although *N. displodere* infects other tissues besides the intestine, feeding is necessary for infection, implying that spores need to first be in the intestinal lumen to infect tissues beyond the intestinal cells. To determine if infection by an epidermal and muscle infecting species was also dependant upon this protein, we infected wild-type and *aaim-1* mutant animals with *N. cider*. Similar to what was observed with *N. parisii* infection, *aaim-1* mutant animals exposed to a high dose of *N. cider* have a reduced prevalence of infection compared to wild-type animals (Fig. S16).

Microsporidia species have an extracellular spore form of a defined morphology which can be used to identify species[13]. *Nematocida* spores have been shown to have a variety of sizes, with the average size of species ranging from 1.3-2.38 µm long and 0.53-1.03 µm wide. Additionally, some species in the *Parisii* group have been shown to have a second, larger, class of spores[15]. To determine spore sizes for the new species we identified, we examined infected animals with stained spores (Fig. S15A-C). This revealed that these species only have a single class of spores, with *N. botruosus* measuring 1.51 x 0.76 µm, *N. cider* measuring 2.4 x 0.67 µm, and *N. ferruginous* measuring 1.72 x 0.6 µm.

Microsporidia has a characteristic infection apparatus known as the polar tube[35]. The length of this tube was previously shown to correlate with tissues infected, where shorter polar tubes (~ 4 µm for *N. parisii*) are seen in species restricted to the intestine, and longer polar tubes (~ 12 µm for *N. displodere*) seen in species that can infect the muscles, neurons, and epidermis. This correlation was hypothesized to be due to the requirement of longer polar tubes to access more distal tissues from the lumen of the intestine[14]. We measured polar tube lengths of several *Nematocida* species using a previously described freeze-thaw approach to trigger spore firing[14] followed by staining with Nile red[36] (Fig. 6E). We observed a range of lengths throughout *Nematocida*, with the shortest being *N. botruosus* with a length of 2.3 µm and the longest being the previously measured *N. displodere* (Fig. 6F)[14].

To understand how various microsporidian phenotypic traits evolve, we arranged our measured attributes onto the phylogenetic tree of *Nematocida (*Fig. 7*)*. We observed all of the *Parisii* group species had a specialized host range and showed specificity for the intestine. In contrast, all of the species in the *Displodere* group, except for *N. botruosus*, had a more generalist host range, suggesting that this property was either lost in *N. botruosus*, or gained after species divergence. Additionally, the *Displodere* group species, *N. displodere*, *N. cider*, and *N. ferruginous*, infected other tissues besides the intestine, suggesting that the ability to infect multiple tissues was most likely present after the divergence of *N. botruosus*, and then lost in *N. homosporus*.

We observed that spore size is flexible throughout *Nematocida* species, with both groups of Nematocida containing species (*N. minor* and *N. botruosus*) exhibiting some of the smallest spores. Additionally, we observed that two classes of spores are present only in the *Parisii* group

and large spore clusters are only present in the *Displodere* group. Finally, we observe flexibility of polar tube length ranging from 2.3 - 12.6 μm. Our data suggests that the last common ancestor of *Nematocida* likely had a relatively short polar tube (less than ~ 4 μm). An increase in polar tube length then occurred in the *Displodere* group after the divergence of *N. botruosus*. This increase in polar tube length correlates with tissue specificity, with the three species with the longest polar tubes all infecting tissues besides the intestine. These results provide further support for microsporidian tube length being a factor in determining which tissues are infected[13]. Together, our results suggest that trait evolution in *Nematocida* is flexible, with gains and loss of attributes common throughout speciation.

Conclusions

To understand genomic evolution of nematode-infecting microsporidia, we sequenced the genomes of nine additional species. We then analyzed these genomes along with four previously sequenced species. We show that core cellular processes, including metabolism, are largely conserved between genera. Our analysis demonstrates that *Enteropsectra* and *Pancytospora* form a sister group to the *Enterocytozoon*, but have not undergone decay of the glycolytic pathway that has occurred in *Enterocytozoon* species[12]. This conservation of metabolism suggests that host metabolic requirements are similar between species and is in contrast to proteins predicted to interface with hosts, which are quite different between different groups of microsporidia[17]. Although we present the largest comparison of protein function between microsporidia species so far, detecting protein function from sequence alone in microsporidia is challenging and thus additional analyses taking advantage of advances in structural prediction are likely to detect highly diverged proteins that would be missed based on sequence similarity alone[9,37,38].

One class of proteins that contributes to diversity between microsporidian species are the large gene families. Previous work identified that all sequenced species of microsporidia contained at least one family, and most families were clade specific[17]. These families were also enriched for secretion signals and transmembrane domains, suggesting that proteins in these families are used to interface with the host[9,17]. Here we show that one of these large gene families, NemLGF1, is present in both *Nematocida* (the *Parisii* group) and *Pancytospora* species. As members of this family are not present in any other microsporidia species, the most likely explanation is that this family was horizontally transferred between a species in each genus, though which genus was the recipient, and which was the donor, is not clear. We also identified a family (NemLGF27) present in *N. ferruginous* which shares similarity to the previously described InterB family found in *Encephalitozoon* species[29]. Although to our knowledge, horizontal transfer of genes between microsporidia proteins has not been previously reported, coinfections of multiple species are often observed, suggesting that these types of events may be more common that previously appreciated[39].

Microsporidia have been shown to display much flexibility in their phenotypic traits[13]. However, determining how traits vary between related species has been challenging as most phylogenetic trees are built from 18S rRNA sequences, resulting in phylogenies that are often of low accuracy[3]. Here, we use genome assemblies to build a high-quality phylogeny for the *Nematocida*. By mapping several phenotypic properties onto this tree, we are able to observe examples of loss and gain of infection properties. As more microsporidian genomes are sequenced, this approach is likely to be useful for further understanding the evolution of microsporidia infection properties and spore characteristics. With our data we show that a generalist host range emerged in the *displodere* group after the divergence of *N. botruosus*. One potential caveat to our measurements of host range is that they are only done with a single strain for each microsporidia and host species[33]. However, we see similar results to what was reported with other *N. parisii* and *N.*

ausubeli strains, and nematode-infecting microsporidia have been observed to mostly infect different host strains at similar levels[15]. Previously, the size of generalist microsporidia genomes were suggested to be smaller than genomes of species that had a more narrow host range[11]. Although the generalist *Nematocida* have some of the smallest genome sizes, they are about the same size as *N. botruosus*, which has a narrow host range. This suggests that other forces are involved in sculpting microsporidia genomes.

Although *C. elegans* has become an important model in which to study many aspects of microsporidia infection, there are currently no tools for genetically perturbating microsporidia that infect this host[40]. Knockdown of genes using RNAi has been demonstrated in microsporidia that infect honey bees, silkworms, fish, and locusts and is becoming a powerful method to investigate the function of microsporidia proteins, including those that are secreted or surface exposed[41–46]. So far, this approach has not been amenable to species that infect *C. elegans*, as *N. parisii* and the other *Nematocida* don't encode the machinery necessary to carry out RNAi[3]. Here we report that *P. epiphaga,* which infects *C. elegans*[15], encodes this machinery, suggesting RNAi may be possible in this species. *C. elegans* may be particularly useful for microsporidian RNAi knockdown, as RNAi of genes in *C. elegans* is highly efficient and can be carried out by feeding bacteria expressing double stranded RNA against the target transcript, resulting in dozens of successful whole genome screens[47]. Additionally, *P. epiphaga* is more closely related to several human pathogens than *N. parisii* and our genomic data will provide a useful resource for further investigations using this species.

Material and methods

Isolation of infected animals

Sampling of nematodes was done similar to as described previously[14]. Briefly, samples of rotting fruit or vegetation were placed on 6-cm NGM plates seeded with 10x saturated cultures of OP50-1 for 16-48 hours. Rotting matter was then removed. *N. ferruginous* was identified using differential interference contrast microscopy to identify animals displaying meronts and/or spores. *N. cider* and *N. botruosus* were identified by growing animals at 21-23°C, washing animals off plates in M9/0.1% Tween-20, and fixing animals in 800 µl acetone. Samples were then stained with Direct yellow 96 (DY96) staining solution (M9, 0.1% SDS, and 20 µg/ml DY96) for 30 min. Samples were resuspended in EverBrite Mounting Medium (Biotium #23002) with DAPI and placed onto microscope slides. Microsporidia containing animals were identified as those containing DY96 stained spores. Nematode host species were determined using sequencing primers as described previously[48].

Removal of contaminating bacteria from microsporidia-infected nematodes

Infected nematodes isolated in this work and previously[15] were grown on 10-cm NGM plates seeded with 10x OP50-1 until populations of worms had ingested all available bacteria. Animals were then washed off plates with M9/0.1% Tween-20 and frozen at -80°C. 2.0 mm zirconia beads were then added and samples vortexed at 3,000 for 5 min in a bead disrupter. The supernatant was then placed onto 6-cm NGM plates containing antibiotics (50 µg/ml carbenicillin, 25 µg/ml kanamycin, 12.5 µg/ml tetracycline, 37.5 µg/ml chloramphenicol, 200 ug/ml cefotaxime, and 100 µg/ml gentamycin) for 24-48 hours. Either the native nematode host strain that the microsporidia species was isolated in or *C. elegans* N2 animals were used to cultivate each species (See Table S1). Mixed populations of nematodes were bleached (~4% sodium hypochlorite and 1 M NaOH) for 2-3 minutes to extract embryos which were hatched at 21°C for 18-24 hours. L1 stage worms were then added to the antibiotic containing plates along with 10X OP50-1. After several days

animals were chunked onto new NGM plates containing antibiotics. After several days animals were chunked onto NGM plates without antibiotics. If no contamination was detected, then samples were used to prepare spores. If not, the above procedure was repeated until there was no contamination.

Preparation and DNA sequencing of microsporidian spores

Spores were prepared similar to as previously described[18]. Briefly, contaminate-free, infected populations of worms were chunked onto 12-48 10-cm OP50-1 seeded NGM plates and grown at 21°C for 5-10 days. After worms had consumed all the OP50-1 bacteria, worms were washed off plates with M9 and frozen at -80°C. Spores were extracted from worms as described above and then filtered through a 5 µm filter (Millipore). The concentration of spore extracts were determined by staining spores with DY96 and counting spores on a sperm counting slide (Cell-VU) using a 20X objective on a Axio Imager.M2 (Zeiss). DNA was extracted using a MasterPure yeast DNA purification kit (Lucigen) according to manufacturer instructions using 10-50 million spores per microsporidia species. DNA libraries were prepared by The Centre for Applied Genomics (TCAG) and each species was sequenced using 2 lanes of a NovaSeq 6000 SP flow cell to produce 250 bp paired-end reads.

Genome assembly & annotation

Adapter sequences ('AGATCGGAAGAG') were removed from paired-end raw reads using cutadapt v21[49]. Leading and trailing low quality (quality < 3) or N bases were removed, low quality bases (quality < 30, except for *P. epiphaga* where 36 was used) were cut using a 4-base sliding window and reads less than 36 bases were dropped using Trimmomatic v0.36[50]. Reads were mapped to the corresponding host genome (except for *N. botruosus* which was mapped to *C. elegans* as well as the *E. coli* genome using bowtie2 v2.3.4.1[51]. Reads were assembled into contigs and scaffolds using Abyss v2.02[52] with a Kmer of 128. Only scaffolds greater than 500 bp were retained. Assemblies were then filtered for contaminants (bacteria and host) using BlobTools v1.0.1[53]. For some samples (Table S2) subsampling was done prior to removing contaminants with BlobTools. Each assembly was run through Redundans v0.14a[54] with a minimum identity value of 0.85, to remove duplication. Assemblies were also filtered for ERTm1[5] contamination if they met the following criteria: 99% identity and 80% query coverage. Additional filtering was done for size and coverage: scaffolds less than 750 bp were removed and those between 750 bp – 1 kbp were removed if they had less than 5X median coverage of the largest 5 scaffolds. NCBI nucleotide blast (BLASTn)[55] was used to filter remaining scaffolds that had >98% identity and >50% query cover to ERTm1/ERTm2 assemblies. Manual filtering of select scaffolds not captured in previous filtering steps was done for six of the samples (See Table S2). Protein coding genes were predicted using Prodigal v2.6.3[56] using translation table 1. Proteins with less than 100 amino acids were kept only if they had a significant (E=0.001) hit to the Uniref90 protein database or PFAM hit using the hmmscan function in HMMER package v3.1b2[57] and E-value cutoff of 0.001. The final list of proteins were annotated with PFAM[58] domains using hmmscan, signal peptides using SignalP v4.1f[59], and transmembrane domains using TMHMM v2.0c[60]. Functional annotation of proteins was also done using BlastKOALA (REF) and InterProScan v5.51-85.0[62] (Table S3).

Phylogeny and genome characterization of microsporidia species

Phylogenetic tree was generated using 45 species. Species whose proteome was downloaded from NCBI are listed in Table S5. The remaining proteomes were predicted from the genomes assembled in this study. In addition, proteins were predicted from two assemblies available on NCBI for the following species: *Metchnikovella incurvata*, and *Enteropsora Canceri*. Orthofinder v2.5.2[24] was used with -M msa option to obtain a MSA species tree with a minimum of 77.8% of species having single copy genes in an orthogroup. Tree was rooted using *Rozella Allomycis*[63] in

FigTree v1.4.4. Protein content, genome size, as well as genome completeness statistics using BUSCO v3.1.0[64] and microsporidia odb9 were computed for each species.

Pathway conservation in microsporidia species

InterProScan v5.51-85.0[62] was run on all species with -goterms option. A database was made with POMBE GO-slim terms (https://www.ebi.ac.uk/QuickGO/slimming) and their descendants (found using QuickGO API using the 'find descendants' option, https://www.ebi.ac.uk/QuickGO/api/index.htmllar#!/gene_ontology/). For each species, protein to GO term annotations from InterProScan were mapped to the above-mentioned database while retaining count of proteins mapping to each GO-term. Since multiple GO terms map to a single GO slim, a unique protein count was obtained for each GO-slim. Using *Rozella allomycis* as the base species, a subset of the POMBE GO-slim terms were obtained and the subset was then searched against the remaining species to compare pathway conservation across species.

Identifying large gene families

OrthoMCL v2.0.9[65] was run using all proteomes and with the following configuration settings: percentMatchCutoff=50 and evalueExponentCutoff=-5, suggested minimum protein length and maximum percent stop codons, and MCL inflation value of 1.5. Paralogous orthogroups were extracted (at least 10 members in a single genome). The genome with the highest number of paralogs for a specific gene family was used as the seed sequences to expand gene families. Seed sequences were searched against each microsporidia genome iteratively using the jackhmmer function in HMMER and an E-value cutoff of 10-5. All resulting large gene families were assessed for signal peptides, transmembrane domains, and PFAM domains. A family was classified as having signal peptides if >50% of the proteins in the family had a signal peptide. The same criteria were applied for transmembrane domains. Families not classified as having signal peptides or transmembrane domains were removed from the analysis. All families with 90% or greater protein overlap were collapsed, with the exception of 1016 cluster which were collapsed with less than 90% overlap in some cases and 1044/1851 which were collapsed based on a 94/75% overlap. We used OrthoMCL only results for families with >5% PFAM representation in either LRR, ZF, or peptidase domains.

Structural modeling of large gene families.

Models of members of large gene families were generated using AlphaFold as implemented in ColabFold[31,32](https://colab.research.google.com/github/sokrypton/ColabFold/blob/main/AlphaFold2.ipynb). Default settings were used for NEPG_02057, and for the other proteins PSI-BLAST[55] was used to identify members and multiple sequence alignments were generated using HHblits (https://toolkit.tuebingen.mpg.de/tools/hhblits)[66]. Alignments of NemLGF1 domains were performed using PyMOL v2.5.3 (https://pymol.org). Structural similarity to solved structures was determined using Dali (http://ekhidna2.biocenter.helsinki.fi/dali/)[67].

Host specificity assays

The following nematode species (strains) were used for infection assays: *C. elegans* (N2), *Caenorhabditis briggsae* (JU2507), *Caenorhabditis nigoni* (JU1422), *Caenorhabditis remanei* (JU2796), *Caenorhabditis tropicalis* (JU1373), *Oscheius tipulae* (JU1505), and *Panagrellus* sp. 2 (AWR79). Mixed populations of nematodes were maintained on 10-cm seeded NGM plates for at least three generations without starvation. Animals were then washed off plates and embryos extracted with bleach as described above, except for *Panagrellus* sp. 2. Synchronized animals of *Panagrellus* sp. 2 were prepared by washing animals with M9 three times and then filtering through a 20 μm nylon filter (millipore SCNY00020). This filtering was then repeated a second time. 400 L1 stage animals of each species were infected with the following microsporidia species (strain [spore amount]): *N. parisii* (JUm1248[3 million]), *N. ausubeli* (ERTm6[0.8 million]), *N. cider*

(AWRm77[4 million]), *N. ferruginous* (LUAm3[20 or 40 million]), and *N. botruosus* (AWRm80[28 million]). Animals and spores were mixed with 400 µl 10X OP50-1 and placed onto 6-cm NGM plates. Plates were dried in a clean cabinet and incubated at 21°C for 96 hours. Animals were then washed off plates, fixed, stained, and placed onto slides as described above. The percentage of animals infected was determined by counting the number of P0 animals that contained newly formed clusters of microsporidia spores.

Infection of *aaim-1* mutants

N2 and *aaim-1* mutants (kea22 and kea28) were infected with *N. cider* (4 million spores) as described above. To quantify pathogen burden within animals (GFP), regions of interest were used to outline individual worms followed by subjection to the "threshold" followed by "measure" tools in FIJI[68].

Tissue specificity determination

Strains of *C. elegans* each expressing GFP specifically in the intestine (ERT413), epidermis (ERT446), or muscle (HC46) were grown on standard NGM plates seeded with OP50-1 to the gravid adult stage. Gravid adults were then harvested in M9 to 15 mL conical tubes, washed three times to reduce bacterial excess, and pelleted by centrifuging at 3000 x g. The pellets were resuspended in 1 mL of M9 buffer and added with 1 mL of bleach solution (1:4 volume ratio of 5M NaOH: 6% NaClO; final concentration of 0.5M NaOH, 2.4% NaClO), incubate for 2 min at room temperature, and washed three times with 13 mL of M9. After the final wash, the solutions containing embryos were incubated overnight on a rotator at room temperature to synchronize to L1 stage.

~1000 L1 stage animals of each strain were plated onto a 6-cm NGM plate with either 1 million *N. ferruginous* or *N. cider* spores. Infection plates were allowed to dry and kept at 20°C. At 3 days post infection, animals were harvested in M9 buffer and fixed with 4% paraformaldehyde in PBST (1x PBS, 0.1% Tween-20) at room temperature for 40 min on a rotator for fluorescent in situ hybridization. Fixed animals were then washed four times, each with 1 mL of PBST, then incubated overnight with a mixture of CAL Fluor Red 610 (CF610)-tagged microsporidian probes, including MicroA-CF610 (CTCTGTCCATCCTCGGCAA), MicroB-CF610 (CTCTCGGCACTCCTTCCTG), MicroD-CF610 (CGAAGGTTTCCTCGGATGTC), and MicroF-CF610 (AGACAAATCAGTCCACGAATT), each at a final concentration of 2.5 ng/mL in hybridization buffer (900 mM NaCl, 20 mM Tris pH 7.5, 0.01% SDS) on a thermal shaker at 46°C, 1000 rpm. After hybridization, animals were washed with FISH wash buffer (hybridization buffer, 5mM EDTA) for three times, each for 30 min, on a thermal shaker at 48°C, 1000 rpm. After washing, animals were rinsed once with PBST, mounted, and imaged with confocal microscope Leica Stellaris 5. Each sample was scanned randomly for 30 infected worms and images were taken in different planes to examine all the infection areas in a single worm. For each strain, infected animals were binned into "yes" or "no" respective to the fluorescent tissue. An infected animal was considered to have a specific tissue type infected if there was at least one infection area colocalized with the tissue marker.

***N. cider* and *N. ferruginous* assays to measure change in host color**

Microsporidia spore size measurements

Infected, fixed, and stained animals were prepared as described above. Images of these infected animals were taken using an 63X objective on an apotome-equipped Axio Imager.M2 (Zeiss).

Images were taken as z-stack maximum intensity projections. These images were analyzed using the straight line tool in ImageJ 1.52[69] to measure the length and width of each spore. Only spores that were not immediately adjacent to other spores were measured. At least 50 spores were measured for each species from a minimum of two infected worms.

Measurements of polar tube lengths

Polar tube lengths were measured for *N. parisii* (ERTm1), *N. ausubeli* (ERTm2), N. minor (JUm1510), N. major (JUm2507), *N. homosporus (*JUm1504*)*, *N. cider* (AWRm77), *N. ferruginous* (LUAm3), and *N. botruosus* (AWRm80). To encourage polar tube extrusion, microsporidia spores in microcentrifuge tubes were exposed to two freeze thaw cycles, after the initial thaw from -80°C. This was done by freezing at -80°C for 10 minutes followed by thawing at room temperature for 10 minutes. Nile red (Sigma-Aldrich 72485) (1mg/ml in acetone) was prepared, sequentially diluted to 100µg/ml in M9, and added to a final concentration of 10µg/ml in freeze-thaw treated spores. Spores were incubated with Nile red for 30 minutes in the dark followed by 2ul of Calcofluor White (Sigma-Aldrich 18909). Polar tubes were imaged at 63x magnification using an Axio Imager.M2 (Zeiss). Polar tube measurements were performed on FIJI[68], using the freehand line tool to trace polar tubes followed by selecting the Analyze → Measure option.

Statistical analysis

Data availability

Taxonomic Summaries.

Phylum: Microsporidia Balbiani 1882

Species: *Nematocida cider* n. sp. Wadi et al. 2022.
LSID

The type strain AWRm77 was found in 2017 inside of its type host nematode *Caenorhabditis* sp. 8 strain AWR77, which was isolated from rotting apples in Stow, Massachusetts, United States. The genome of this microsporidia strain has been sequenced and deposited in Genbank under accession JALPNA000000000. This species has been observed to infect the intestinal, muscle and epidermal tissues of *C. elegans*. Experimental infection has been observed in *C. elegans* (N2), *Caenorhabditis briggsae* (JU2507), *Caenorhabditis nigoni* (JU1422), *Caenorhabditis remanei* (JU2796*)*, *Caenorhabditis tropicalis* (JU1373), *Oscheius tipulae* (JU1505), and *Panagrellus* sp. 2 (AWR79). Transmission occurs horizontally. The spores are ovoid and measure as 2.4 x 0.67 µm. The fired polar tube measures 8.3 µm. This species is named after the brown color the animals display after being infected for several days and this color resembles that of cider donuts available in the area where the specimen was found.

Species: *Nematocida ferruginous* n. sp. Wadi et al. 2022.

LSID

The type strain LUAm1 was found in 2017 inside of its type host nematode *C. elegans* strain LUA1, which was isolated from a rotting *Heracleum* sp. stem in Santeuil, France (GPS coordinates 49.12138616666667,1.951088333333333). The genome of this strain has been sequenced and deposited in Genbank under accession JALPMW000000000. This species has been observed to infect the muscle and epidermal tissues of *C. elegans*. Experimental infection has been observed in *C. elegans* (N2), *Caenorhabditis briggsae* (JU2507), *Caenorhabditis remanei* (JU2796), *Caenorhabditis tropicalis* (JU1373), *Oscheius tipulae* (JU1505). Transmission occurs horizontally and is likely via a fecal-oral route. The spores are ovoid and measure as 1.72 x 0.6 µm. The fired polar tube measures 6.2 µm. This species is named after the rust-like brown color the animals display after being infected for several days.

Species: *Nematocida botruosus* n. sp. Wadi et al. 2022.
LSID

The type strain AWRm80 was found in 2018 inside of its type host *Panagrellus* sp. 2 strain AWR80, which was isolated from rotting apples in Georgina, Ontario, Canada. The genome of this strain has been sequenced and deposited in Genbank under accession JALPMX000000000. This species has only been observed to infect the intestine of this animal and transmission occurs horizontally. The spores are ovoid and measure as 1.51 x 0.76 µm. The fired polar tube measures 2.3 µm. This species was named after the prominent large spore clusters formed.

Acknowledgements
We thank X and Y for providing helpful comments on the manuscript. We thank Marie-Anne Félix for providing previously published microsporidia species and for providing support to R. L. during isolation of *N. ferruginous*. This work was supported by a Canadian Institutes of Health Research grant no. 400784 (to A.R.) and an Alfred P. Sloan Research Fellowship FG2019-12040 (to A.R.). Some strains were provided by the CGC, which is funded by NIH Office of Research Infrastructure Programs (P40 OD010440).

Author contributions: L.W. and A.R. conceived of the project. L.W. performed all genomic analysis. N. I. contributed code to the genomic analysis. T.T., H.T.E.J., R. L, and A. R. performed experiments. R.L. and A. R. provided mentorship and acquisition of funding. L.W and A.R. co-wrote the paper with edits from T.T., H.T.E.J., N.I., and R. L.

Competing Interests: The authors declare that they have no competing interests.

Figures

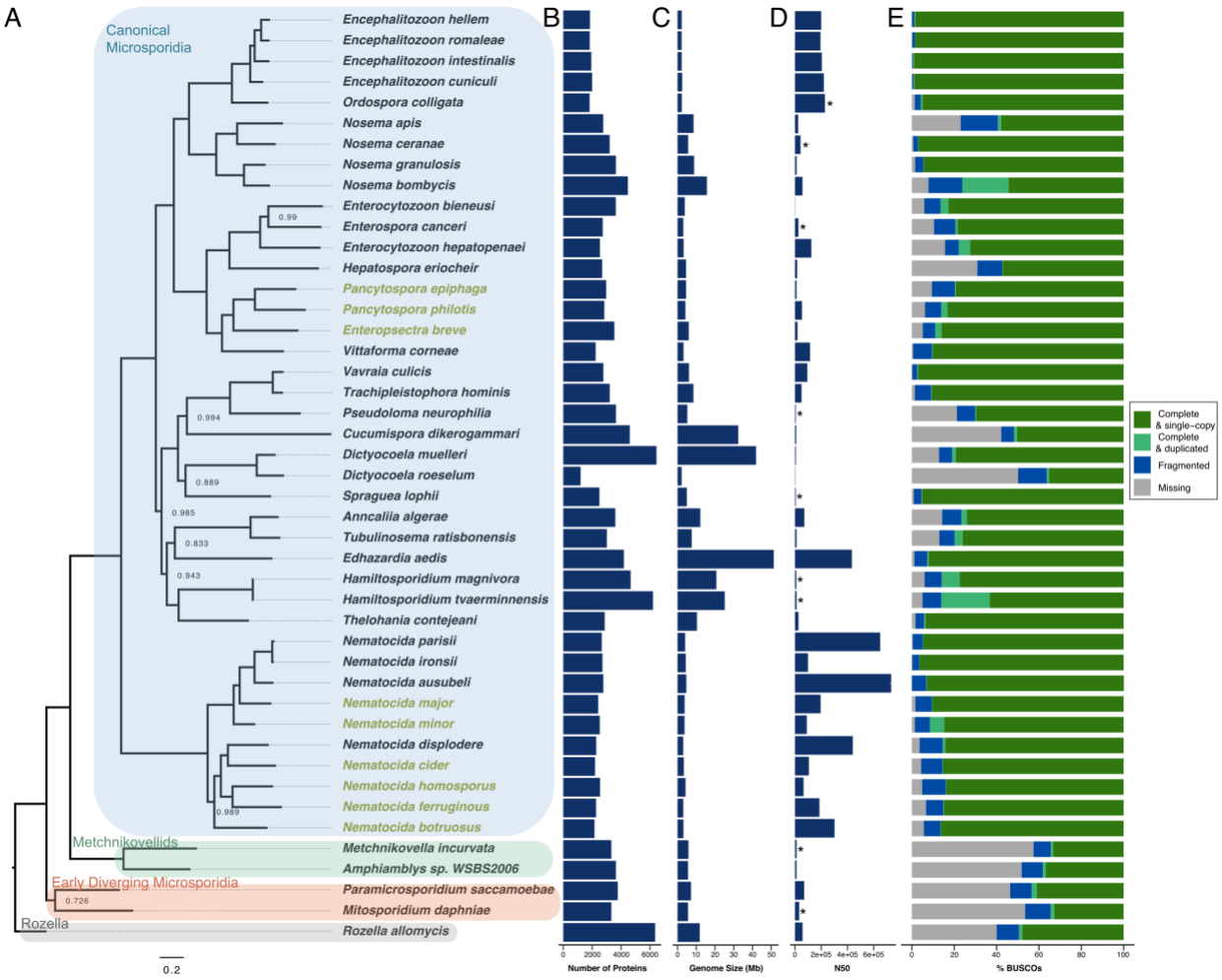

Fig. 1. Phylogeny and properties of microsporidia genomes. (A) Phylogenetic trees of 44 microsporidia species and the outgroup *Rozella allomycis* was constructed using Orthofinder. Bootstrap values less than 1.0 are indicated at each node. Scale indicates changes per site. Previously sequenced species are shown in black and newly sequenced genomes presented in this paper are shown in yellow. Species are grouped into four classes (Rozella, early diverging microsporidia, metchnikovellids, and canonical microsporidia) as previously described[3]. **(B)** number of predicted proteins encoded by each genome. **(C)** Genome assembly size of each species **(D)** Genome assembly N50 values. The scaffold N50 value is shown, except for those indicated by an * which are the contig N50 values. **(E)** Prescence of conserved microsporidian orthologs measured as the percent BUSCOs present in each genome.

Fig. 2. Conservation of protein function across microsporidia genomes. Membership of proteins from *R. allomycis* and 40 microsporidia species in Pombe GO-slim categories was determined. The number of proteins from each species determined to belong to each GO slim category is shown as a heatmap with GO-slim categories in rows and species in columns. Only GO slim categories that contain at least one protein from any of these species are shown. Legend for the number of proteins in each cell is shown at the right. Phylogenetic tree, shown at bottom, was constructed using Orthofinder. Several species (*Pseudoloma neurophilia, Dictyocoela roeselum*, *Cucumispora dikerogammari*, and *Nosema apis*) were excluded on the basis of being poorer quality genome assemblies (See Fig. 1).

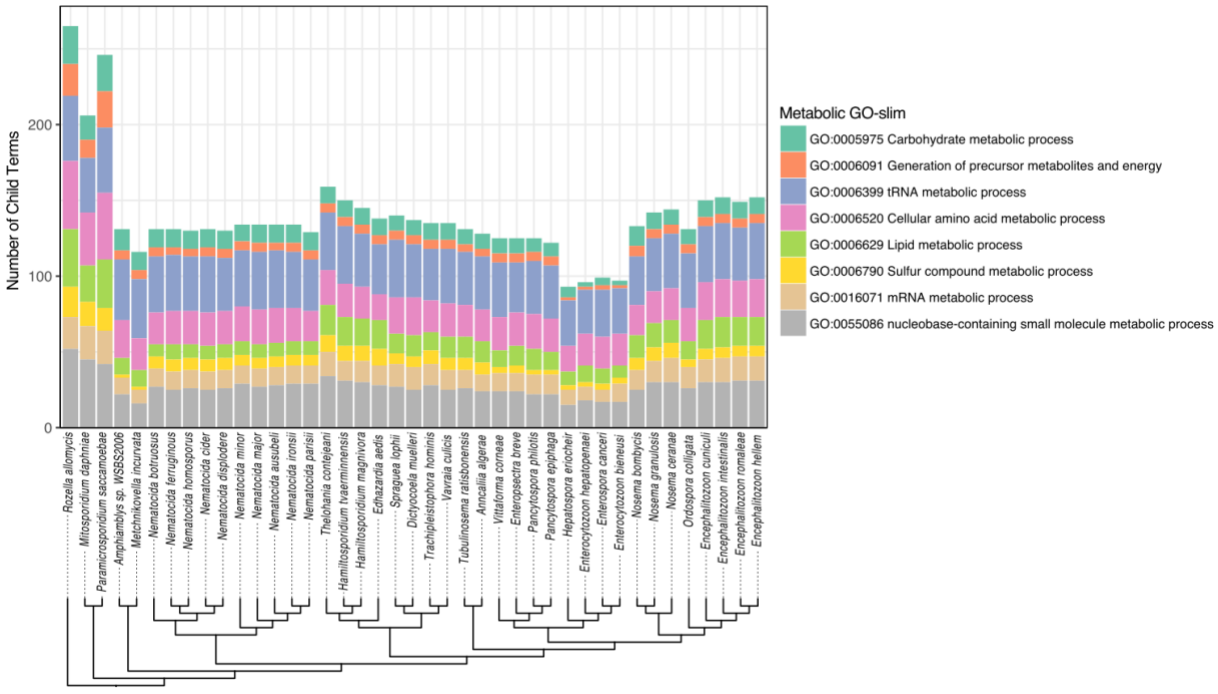

Fig. 3. Prescence of metabolic enzymes in microsporidia species. Membership of proteins from *R. allomycis* and 40 microsporidia species in eight GO-slim metabolic categories was determined. The number of proteins from each species determined to belong to each category is shown as a stacked bar graph, with the legend for each metabolic Go-slim shown at the right. Phylogenetic tree, shown at bottom, was constructed using Orthofinder. Several species (*Pseudoloma neurophilia, Dictyocoela roeselum*, *Cucumispora dikerogammari*, and *Nosema apis*) were excluded on the basis of being poorer quality genome assemblies (See Fig. 1).

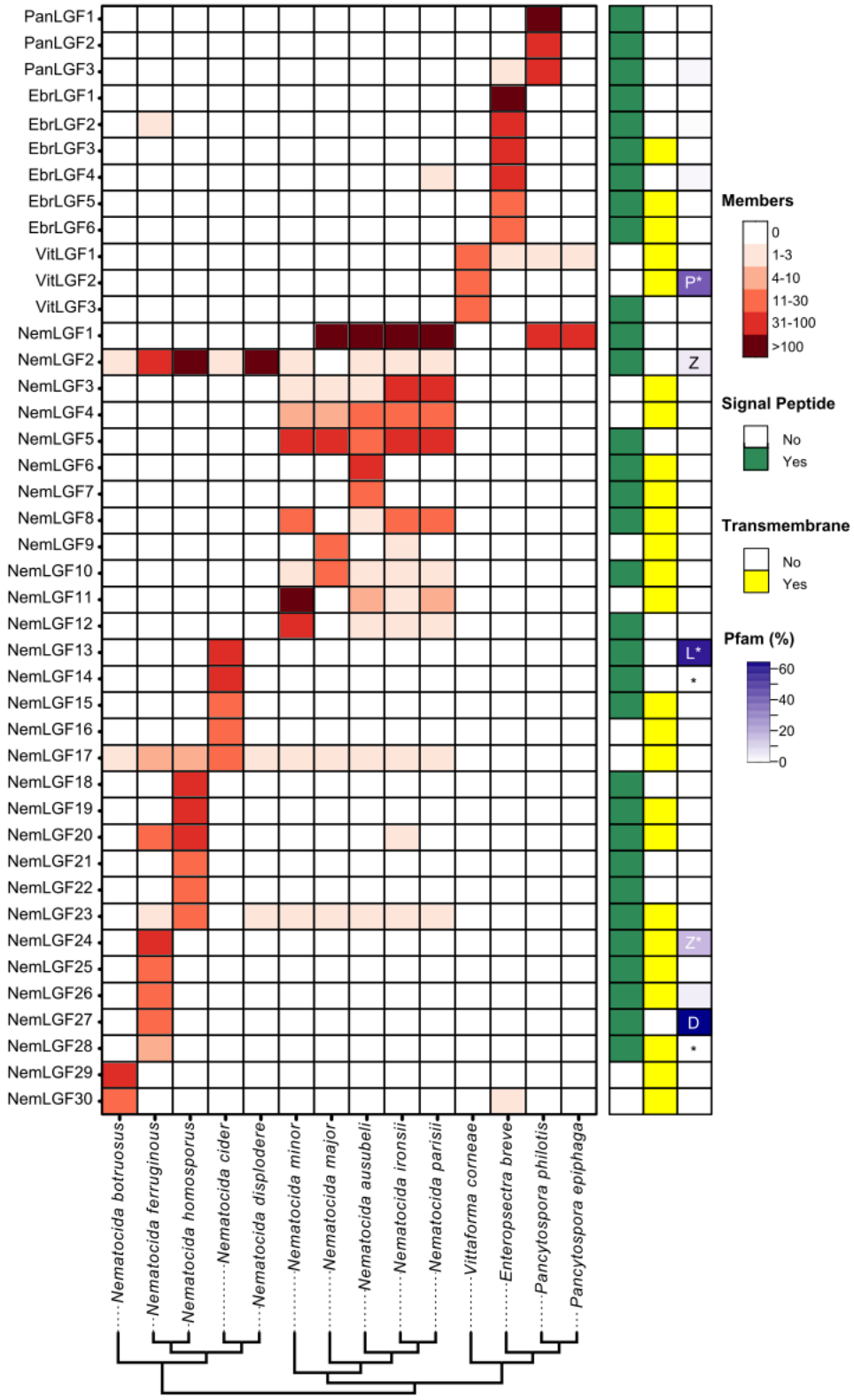

Fig. 4. Nematode infecting microsporidia contain many diverse large gene families.
The number of members of each large gene family (listed in rows) in each species (listed in columns) is shown as a heatmap according to the scale at the top right. The presence of predicted

signal peptides (green), transmembrane domains (yellow), or Pfam domains (purple gradient) are shown to the right. Families containing the Pfam domains peptidase (P), Zinc finger (Z), LRR(L) and DUF1609(D) are indicated. Families that were determined using OrthoMCL are indicated with *. Species are arranged according to the phylogenetic tree shown in Figure 1.

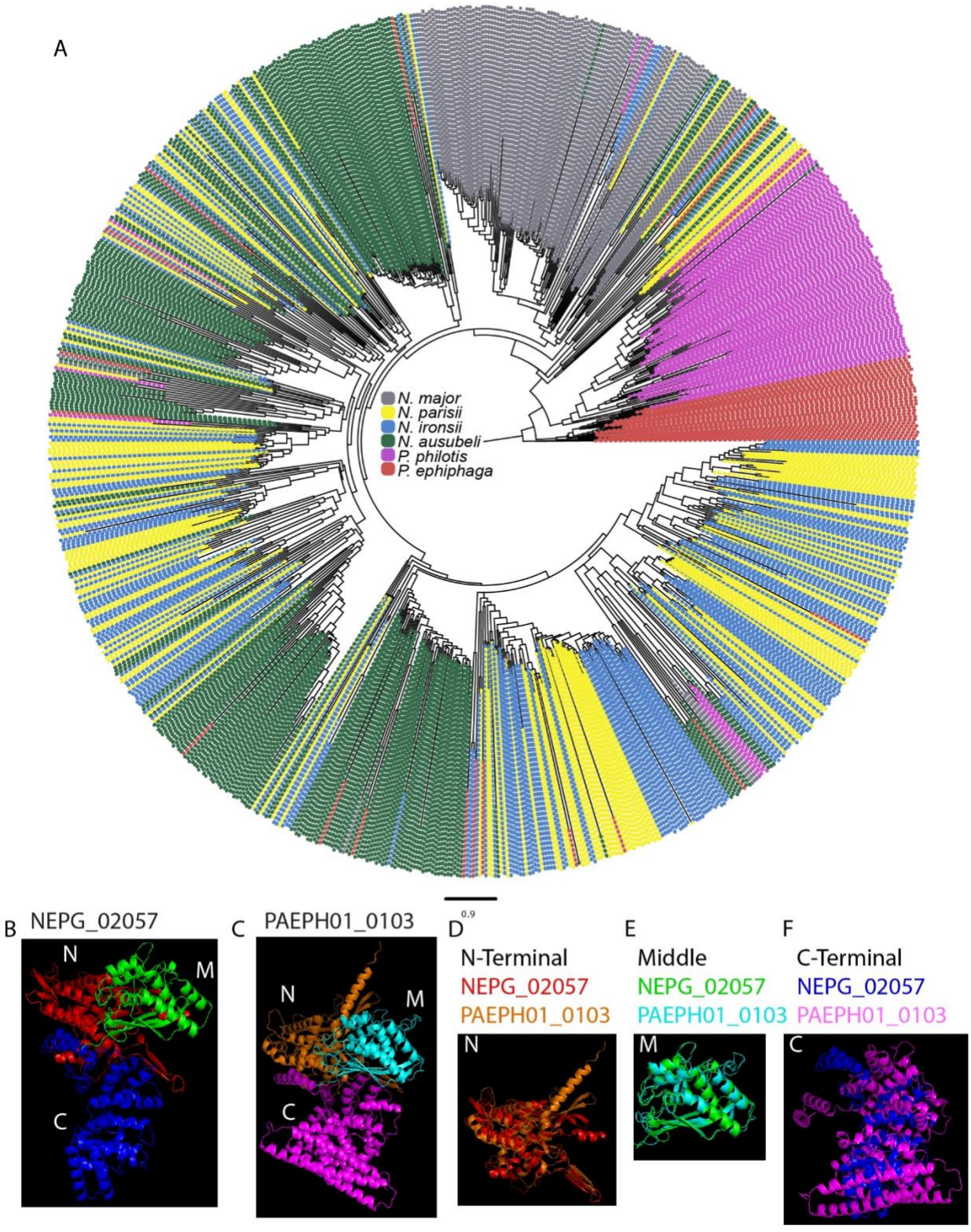

Fig. 5. The large gene family NemLGF1 has likely been horizontally transferred between genera. (A) Phylogenetic tree of NemLGF1 family members, colored by species according to the legend in the middle of the tree. Scale indicates changes per site. (B-C) AlphaFold models of *N.*

parisii NEPG_02057 (B) and *P. ephiphaga* PAEPH01_0103 (C). (D-F) Aligned structures of the N-terminal (D), middle (E), and C-terminal (F) domains. N, N-terminal. M, middle. C, C-terminal.

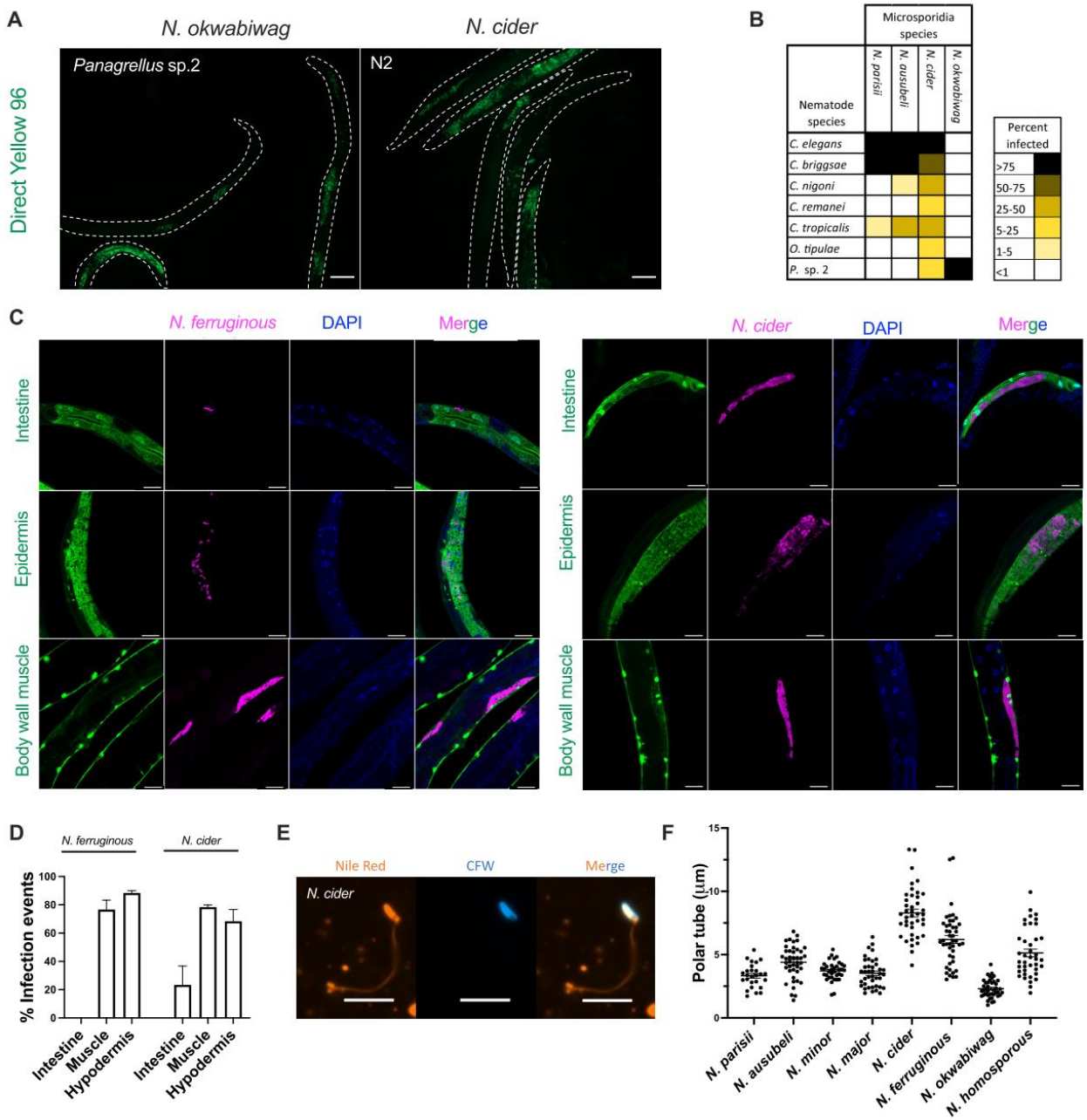

Fig. 6. Determination of host range, tissue specificity, and polar tube length of *Nematocida* species. (A-B) Seven species of L1 stage nematodes were infected with the following species (spore concentration): *N. parisii* (3 million), *N. ausubeli* (0.8 million), *N. cider* (4 million), and *N. botruosus* (28 million). After 96 hours of incubation with spores, animals were fixed and stained with direct yellow 96. **(A)** Representative images of *C. elegans* infected with *N. cider* and *Pangrellus* sp.2 infected with *N. botruosus*. Scale bars, 100 µm. **(B)** Percent of each population

of animals infected with each species of microsporidia. Data is displayed as a heat map with host species in rows, microsporidia species in columns, and the value of each cell being the percent of each population that displayed newly formed microsporidia spores. Legend is displayed on the right. Data shown are the average of two biological replicates with 20-391 animals counted for each sample. **(C-D)** L1 stage *C. elegans* strains expressing GFP in either the intestine, epidermis, or body wall muscle were infected with either 1 million *N. cider* or *N. ferruginous* spores. After 72 hours animals were fixed and stained with an *Nematocida* 18S RNA fish probe and DAPI. Note that for *N. ferruginous* infection of the GFP-intestinal strain (top), that the infection is seen to lie outside of the GFP indicating a lack of intestinal infection. **(C)** Representative images of infection of each species in each strain. Scale bars, 20 μm. **(D)** The percent of the population of each strain containing microsporidia infection within the marked tissue. Data are from over 2 biological replicates and a total of 60 animals examined for each condition. Graphs show mean with SD error bars. **(E-F)** Spores of *Nematocida* species were induced to fire through repeated freeze thawing and then stained with nile red and calcofluor white. **(E)** Representative image of a stained *N. cider* polar tube. Scale bars, 5 μm. **(F)** The length of polar tubes of each species is displayed. 26-41 polar tubes were measured for each species. Mean ± SEM represented by horizontal bars

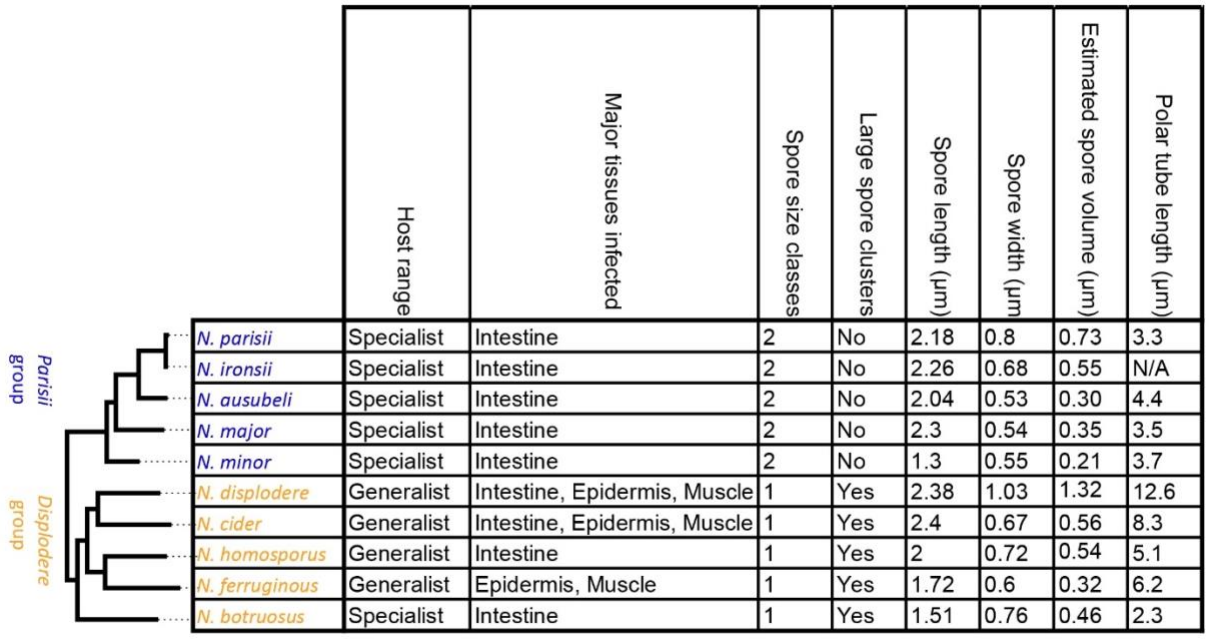

	Host range	Major tissues infected	Spore size classes	Large spore clusters	Spore length (μm)	Spore width (μm	Estimated spore volume (μm)	Polar tube length (μm)
N. parisii	Specialist	Intestine	2	No	2.18	0.8	0.73	3.3
N. ironsii	Specialist	Intestine	2	No	2.26	0.68	0.55	N/A
N. ausubeli	Specialist	Intestine	2	No	2.04	0.53	0.30	4.4
N. major	Specialist	Intestine	2	No	2.3	0.54	0.35	3.5
N. minor	Specialist	Intestine	2	No	1.3	0.55	0.21	3.7
N. displodere	Generalist	Intestine, Epidermis, Muscle	1	Yes	2.38	1.03	1.32	12.6
N. cider	Generalist	Intestine, Epidermis, Muscle	1	Yes	2.4	0.67	0.56	8.3
N. homosporus	Generalist	Intestine	1	Yes	2	0.72	0.54	5.1
N. ferruginous	Generalist	Epidermis, Muscle	1	Yes	1.72	0.6	0.32	6.2
N. botruosus	Specialist	Intestine	1	Yes	1.51	0.76	0.46	2.3

Fig. 7. *Nematocida* phenotypic properties. Table of phenotypic properties for *Nematocida* species, arranged according to the phylogenetic tree (left) determined in Fig. 1. Host range, tissues infected, spore size classes, presence of large spore clusters, spore size, and polar tube length was determined in this paper and from several previously published studies[14–16]. Estimated spore volume was calculated for spore length and width measurements as previously described[13]. N/A, Not available.

Supplemental material:

Fig. S1. Similarity of *N. ferruginous* assemblies.
Fig. S2. Phylogenetic tree of *Nematocida* species.
Fig. S3. Genome size and number of encoded proteins are correlated in nematode-infecting microsporidia.
Fig. S4. Conservation of carbohydrate metabolic processes across microsporidia genomes.
Fig. S5. Conservation of generation of precursor metabolites and energy pathways across microsporidia genomes.
Fig. S6. Conservation of tRNA metabolic processes across microsporidia genomes.
Fig. S7. Conservation of cellular amino acid metabolic processes across microsporidia genomes.
Fig. S8. Conservation of lipid metabolic processes across microsporidia genomes.
Fig. S9. Conservation of sulfur compound metabolic processes across microsporidia genomes.
Fig. S10. Conservation of mRNA metabolic processes across microsporidia genomes.
Fig. S11. Conservation of nucleobase-containing small molecule metabolic processes across microsporidia genomes
Fig. S12. Minimal ancestral deviation analysis of NEMLGF1 tree root.
Fig. S13. Structural models of nematode-infecting microsporidia large gene families.
Fig. S14. *N. ferruginous* infects multiple host species.
Fig. S15. Spore formation observed in the intestine for *N. botruosus* and throughout the animal for *N. cider* and *N. ferruginous*.
Fig. S16. AAIM-1 is necessary for efficient infection by *N. cider.*

Table S1. Summary of microsporidia species and their hosts.
Table S2. Methods used to assemble each microsporidia genome.
Table S3. Annotation of microsporidia genomes.
Table S4. Summary of genome assembly statistics.
Table S5. List of genome assemblies used.
Table S6. RNAi pathway proteins in *Pancytospora* and *Enteropsectra.*
Table S7. List of large gene family proteins.
Table S8. NemLGF27 proteins present in other microsporidia species.

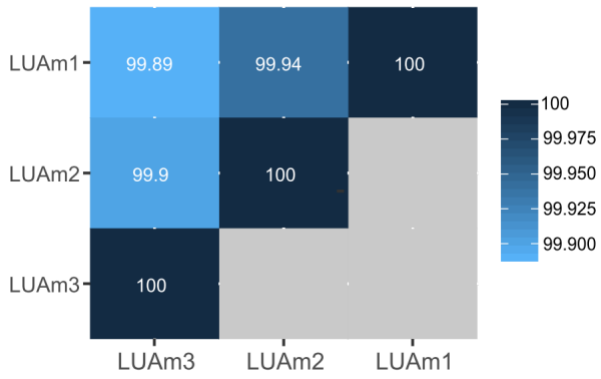

Fig. S1. Similarity of *N. ferruginous* assemblies.
The pairwise nucleotide identify of the three *N. ferruginous* assemblies (LUAm1-3) were calculated and displayed as heat map. The similarity between each assembly is colored according to the legend at the right.

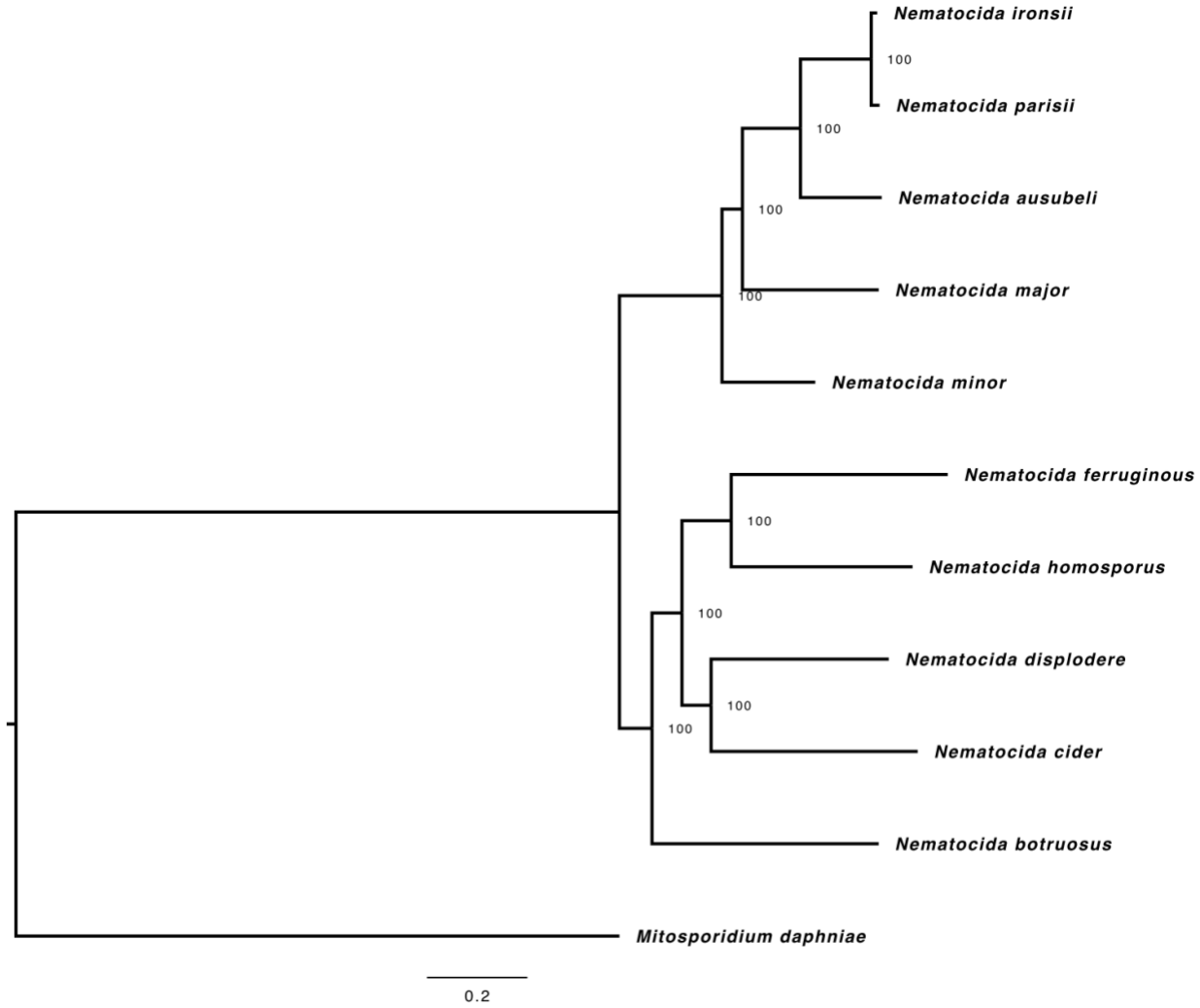

Fig. S2. Phylogenetic tree of *Nematocida* species. The phylogeny of 10 Nematocida species was determined from X single copy orthologs identified using OrthoMCL. Phylogenetic tree was generated using RaxML. *M. daphniae* is shown as an outgroup. Bootstrap values are indicated at each node. Scale indicates changes per site.

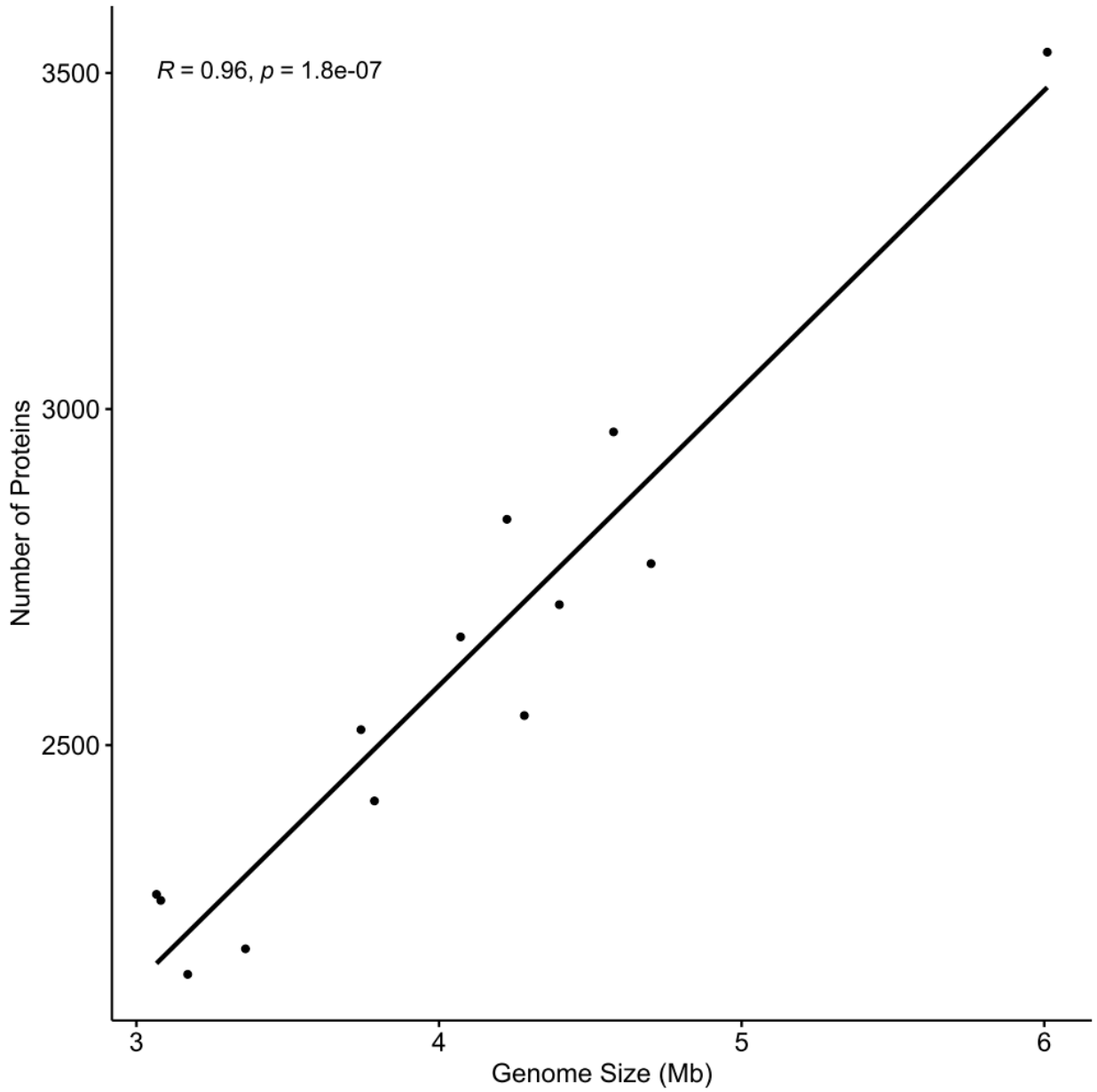

Fig. S3. Genome size and number of encoded proteins are correlated in nematode-infecting microsporidia. The correlation between genome size and protein number in 13 nematode-infecting microsporidia genomes is shown as a scatter plot. The R^2 and p-value of the linear regression are shown in the top left.

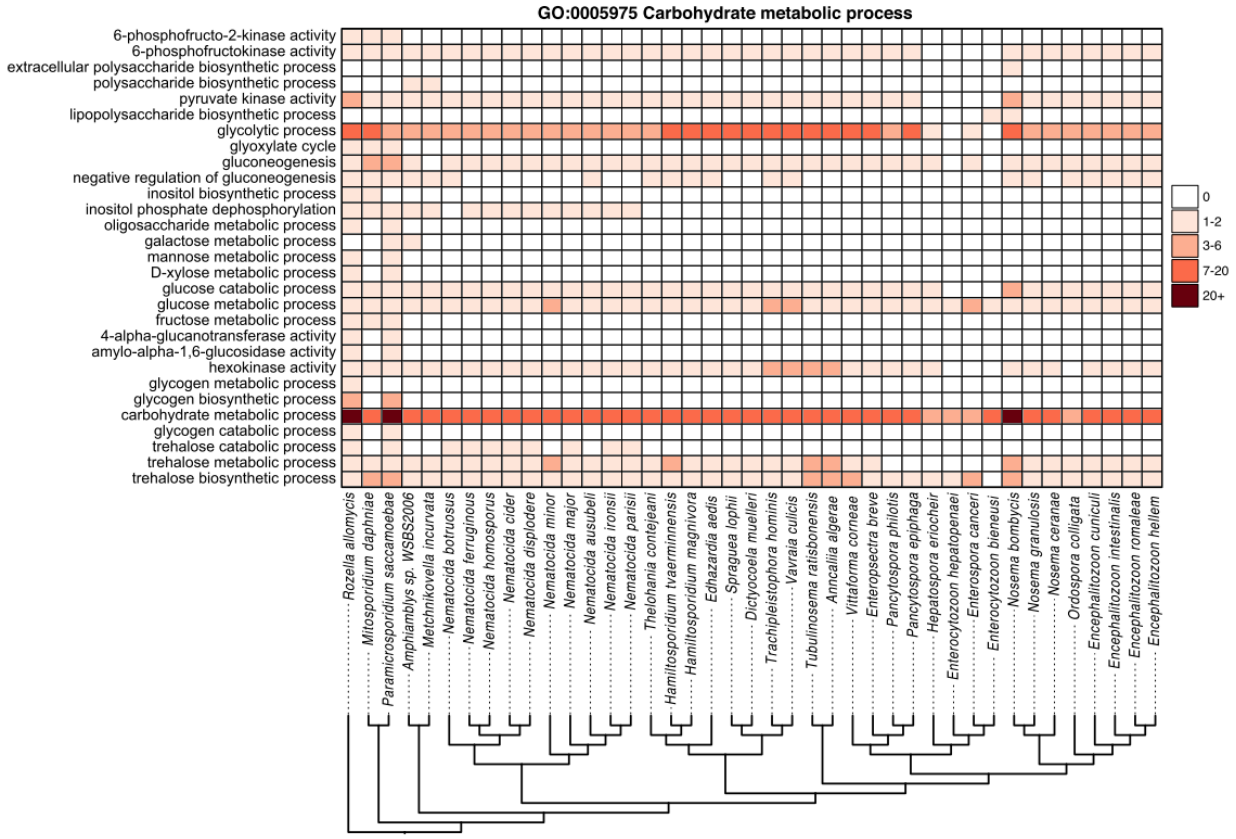

Fig. S4. Conservation of carbohydrate metabolic processes across microsporidia genomes. Membership of proteins from *R. allomycis* and 40 microsporidia species in descendant GO terms from the Pombe GO-slim category "carbohydrate metabolic process" was determined. The number of proteins from each species determined to belong to each Go term is shown as a heatmap with GO-slim categories in rows and microsporidia species in columns. Only descendant GO terms that contain at least one protein from any of these species is shown. Legend for the number of proteins in each cell is shown at the right. Phylogenetic tree, shown at bottom, was constructed using Orthofinder. Several species (*Pseudoloma neurophilia, Dictyocoela roeselum*, *Cucumispora dikerogammari*, and *Nosema apis*) were excluded on the basis of being poorer quality genome assemblies (See Fig. 1).

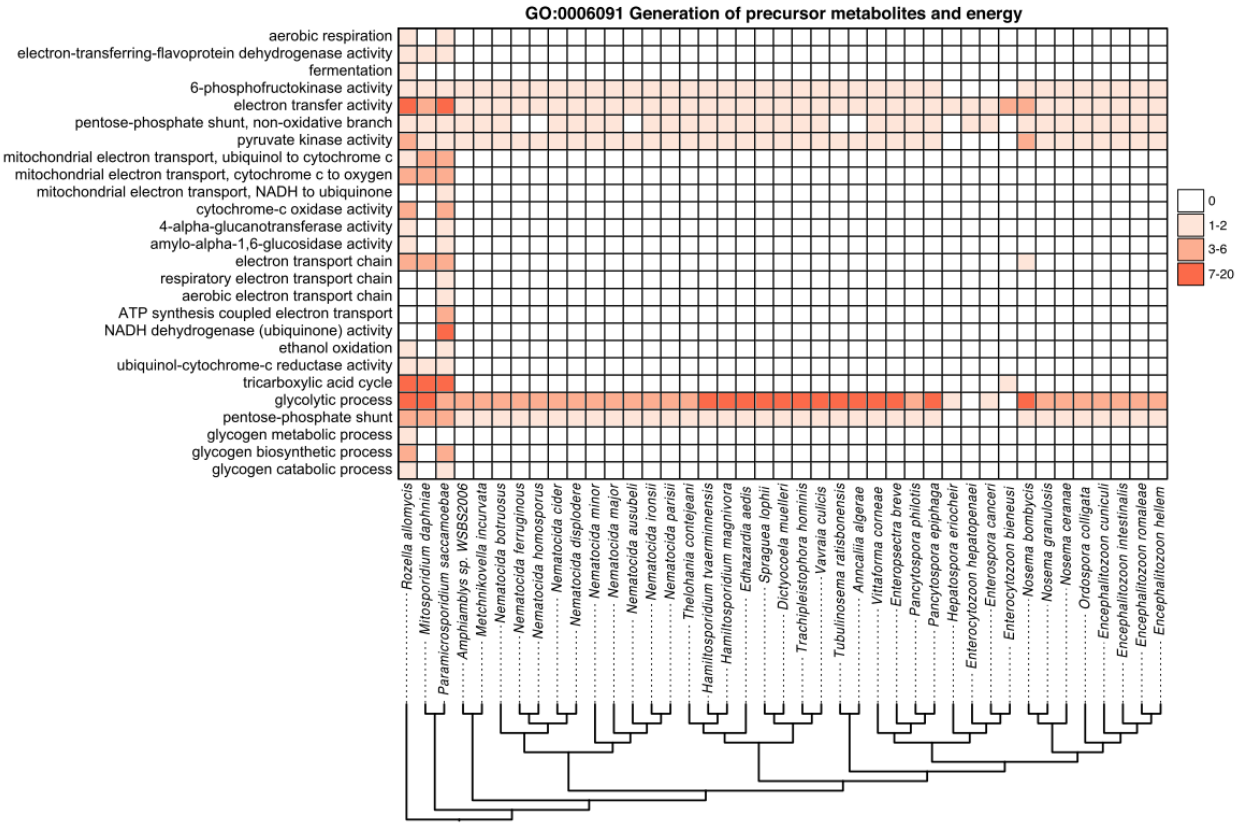

Fig. S5. Conservation of generation of precursor metabolites and energy pathways across microsporidia genomes. Membership of proteins from *R. allomycis* and 40 microsporidia species in descendant GO terms from the Pombe GO-slim category "generation of precursor metabolites and energy" was determined. The number of proteins from each species determined to belong to each Go term is shown as a heatmap with GO-slim categories in rows and microsporidia species in columns. Only descendant GO terms that contain at least one protein from any of these species is shown. Legend for the number of proteins in each cell is shown at the right. Phylogenetic tree, shown at bottom, was constructed using Orthofinder. Several species (*Pseudoloma neurophilia, Dictyocoela roeselum*, *Cucumispora dikerogammari*, and *Nosema apis*) were excluded on the basis of being poorer quality genome assemblies (See Fig. 1).

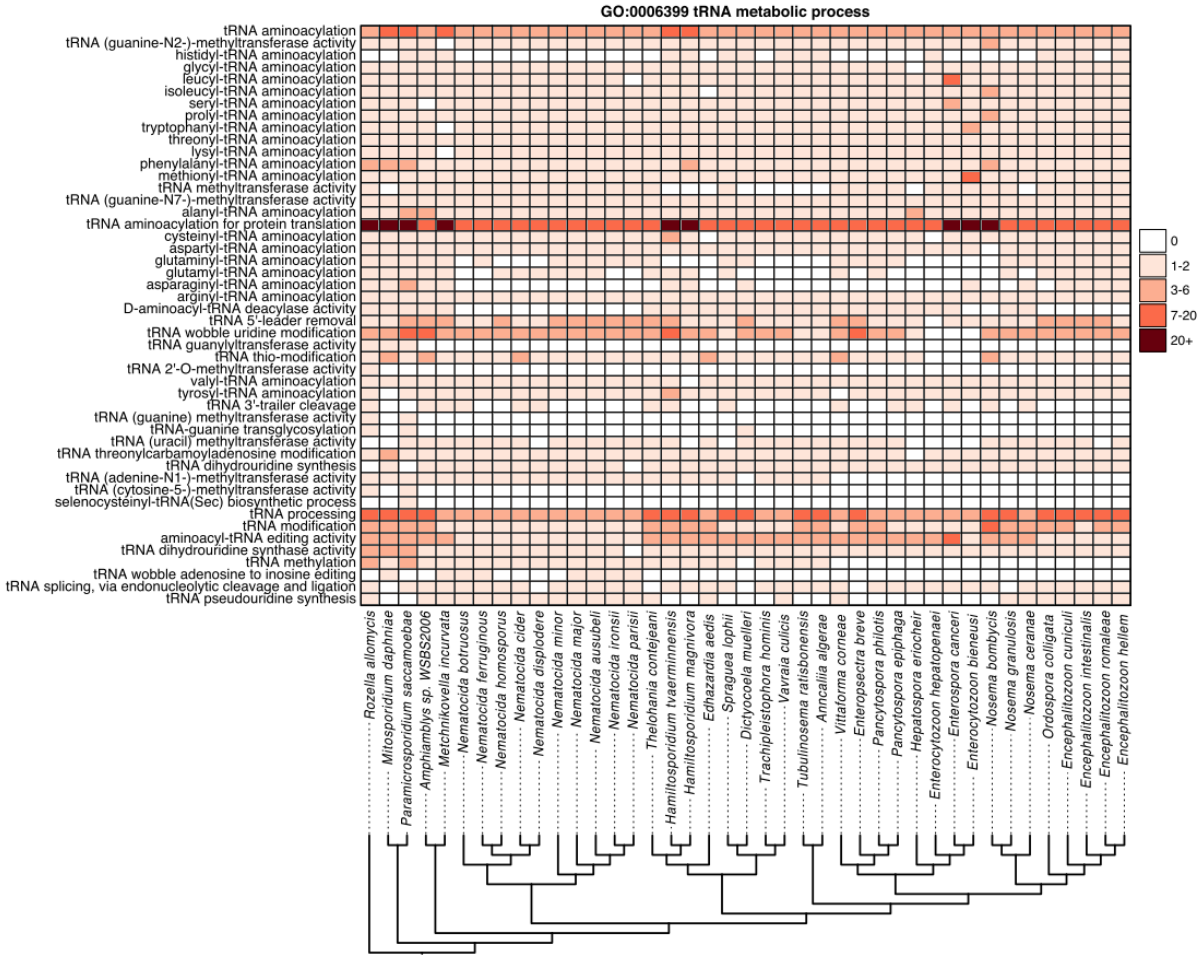

Fig. S6. Conservation of tRNA metabolic processes across microsporidia genomes. Membership of proteins from *R. allomycis* and 40 microsporidia species in descendant GO terms from the Pombe GO-slim category "tRNA metabolic process" was determined. The number of proteins from each species determined to belong to each Go term is shown as a heatmap with GO-slim categories in rows and microsporidia species in columns. Only descendant GO terms that contain at least one protein from any of these species is shown. Legend for the number of proteins in each cell is shown at the right. Phylogenetic tree, shown at bottom, was constructed using Orthofinder. Several species (*Pseudoloma neurophilia, Dictyocoela roeselum*, *Cucumispora dikerogammari*, and *Nosema apis*) were excluded on the basis of being poorer quality genome assemblies (See Fig. 1).

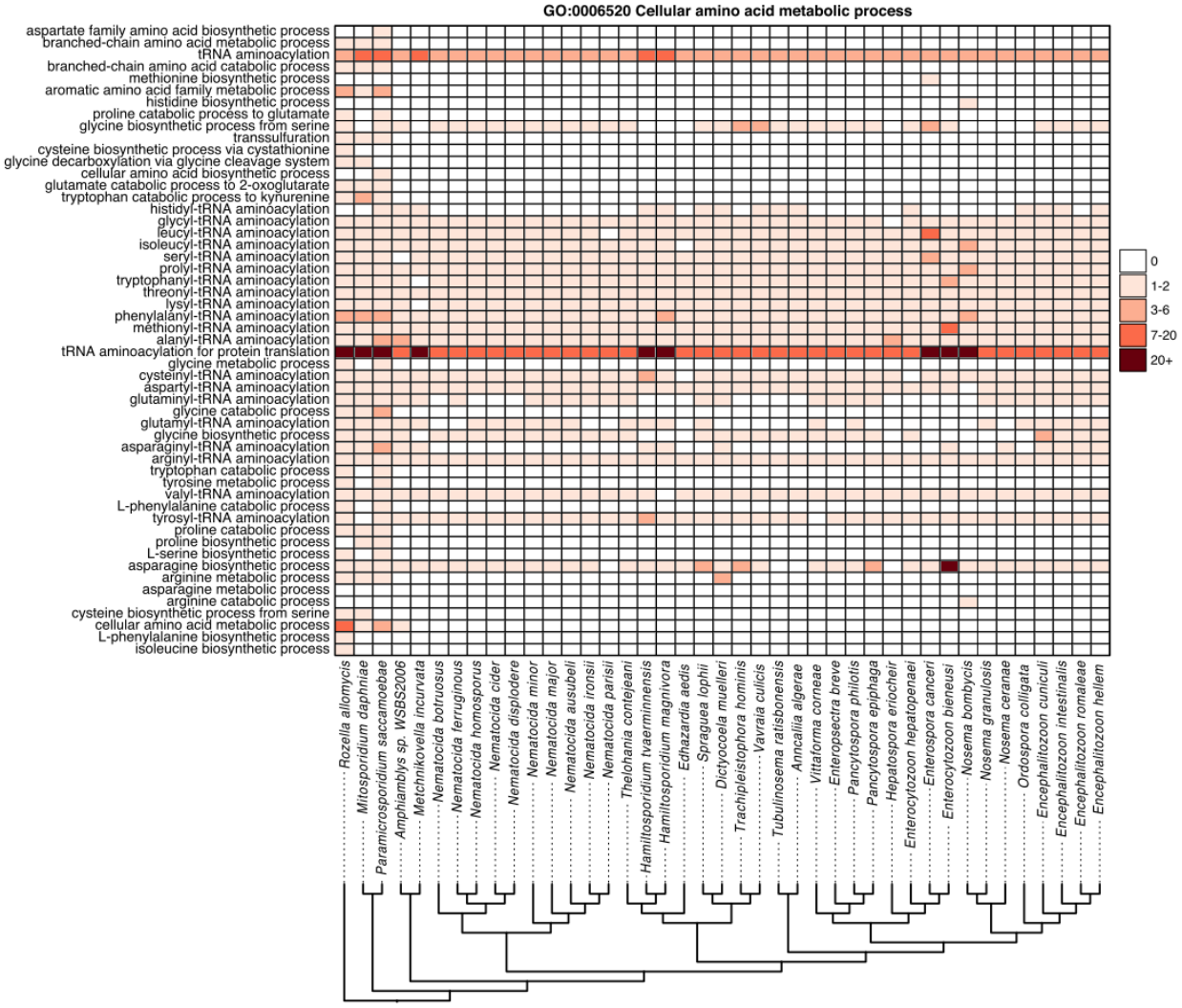

Fig. S7. Conservation of cellular amino acid metabolic processes across microsporidia genomes. Membership of proteins from *R. allomycis* and 40 microsporidia species in descendant GO terms from the Pombe GO-slim category "cellular amino acid metabolic process" was determined. The number of proteins from each species determined to belong to each Go term is shown as a heatmap with GO-slim categories in rows and microsporidia species in columns. Only descendant GO terms that contain at least one protein from any of these species is shown. Legend for the number of proteins in each cell is shown at the right. Phylogenetic tree, shown at bottom, was constructed using Orthofinder. Several species (*Pseudoloma neurophilia, Dictyocoela roeselum*, *Cucumispora dikerogammari*, and *Nosema apis*) were excluded on the basis of being poorer quality genome assemblies (See Fig. 1).

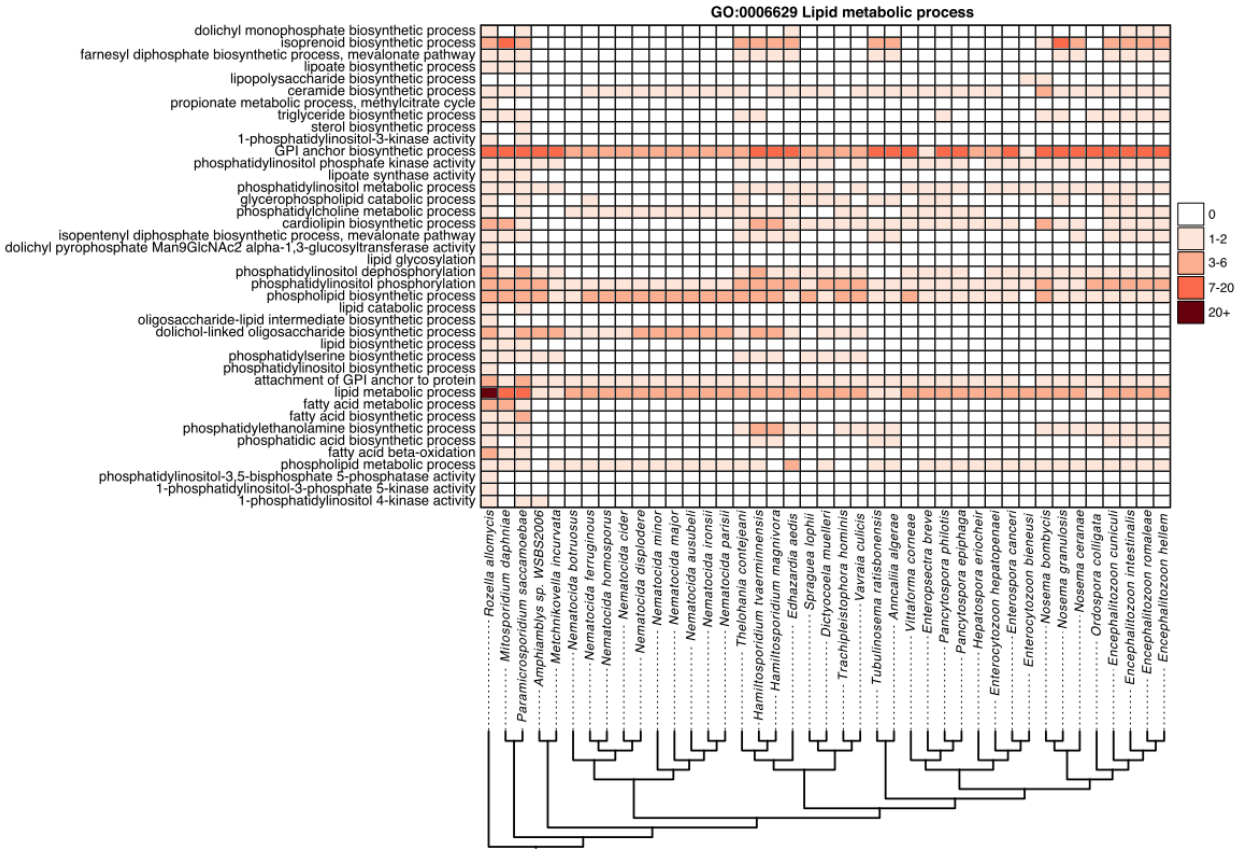

Fig. S8. Conservation of lipid metabolic processes across microsporidia genomes. Membership of proteins from *R. allomycis* and 40 microsporidia species in descendant GO terms from the Pombe GO-slim category “lipid metabolic process” was determined. The number of proteins from each species determined to belong to each Go term is shown as a heatmap with GO-slim categories in rows and microsporidia species in columns. Only descendant GO terms that contain at least one protein from any of these species is shown. Legend for the number of proteins in each cell is shown at the right. Phylogenetic tree, shown at bottom, was constructed using Orthofinder. Several species (*Pseudoloma neurophilia, Dictyocoela roeselum*, *Cucumispora dikerogammari*, and *Nosema apis*) were excluded on the basis of being poorer quality genome assemblies (See Fig. 1).

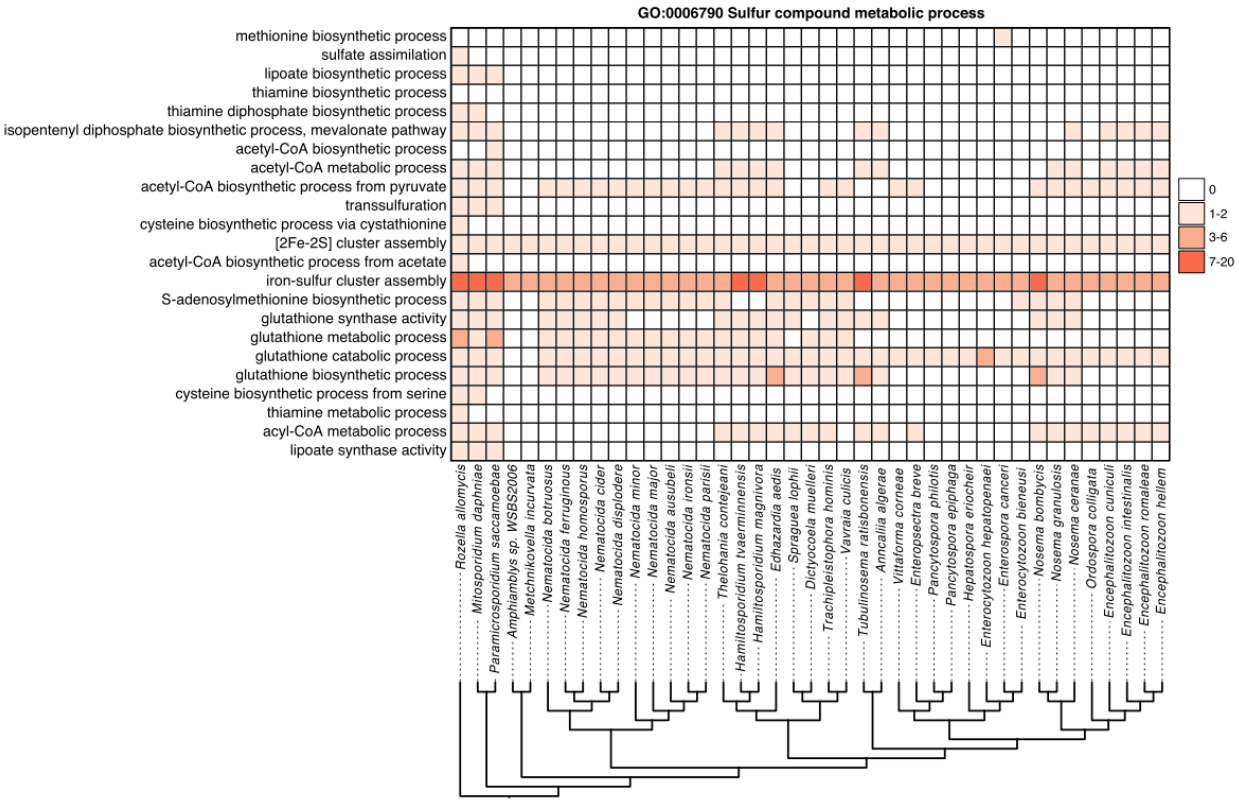

Fig. S9. Conservation of sulfur compound metabolic processes across microsporidia genomes. Membership of proteins from *R. allomycis* and 40 microsporidia species in descendant GO terms from the Pombe GO-slim category “sulfur compound metabolic process” was determined. The number of proteins from each species determined to belong to each Go term is shown as a heatmap with GO-slim categories in rows and microsporidia species in columns. Only descendant GO terms that contain at least one protein from any of these species is shown. Legend for the number of proteins in each cell is shown at the right. Phylogenetic tree, shown at bottom, was constructed using Orthofinder. Several species (*Pseudoloma neurophilia, Dictyocoela roeselum*, *Cucumispora dikerogammari*, and *Nosema apis*) were excluded on the basis of being poorer quality genome assemblies (See Fig. 1).

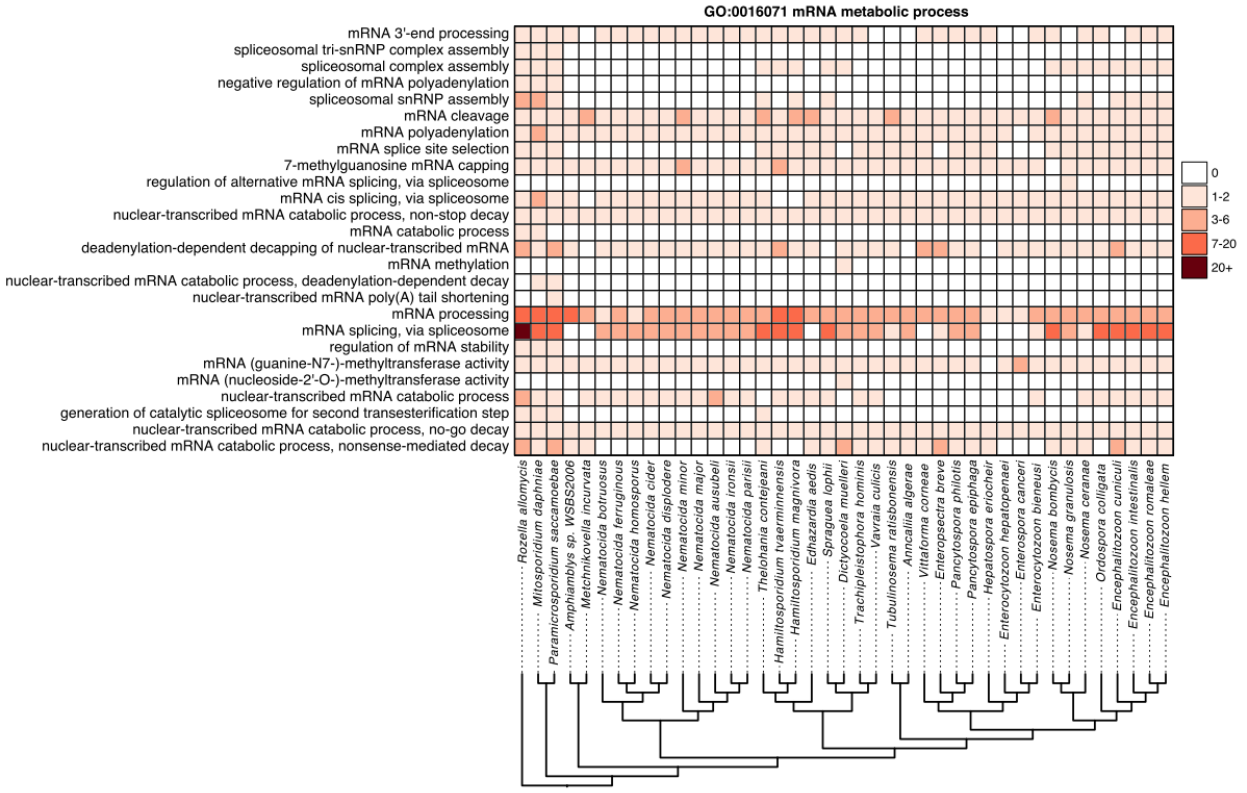

Fig. S10. Conservation of mRNA metabolic processes across microsporidia genomes. Membership of proteins from *R. allomycis* and 40 microsporidia species in descendant GO terms from the Pombe GO-slim category “mRNA metabolic process” was determined. The number of proteins from each species determined to belong to each Go term is shown as a heatmap with GO-slim categories in rows and microsporidia species in columns. Only descendant GO terms that contain at least one protein from any of these species is shown. Legend for the number of proteins in each cell is shown at the right. Phylogenetic tree, shown at bottom, was constructed using Orthofinder. Several species (*Pseudoloma neurophilia, Dictyocoela roeselum*, *Cucumispora dikerogammari*, and *Nosema apis*) were excluded on the basis of being poorer quality genome assemblies (See Fig. 1).

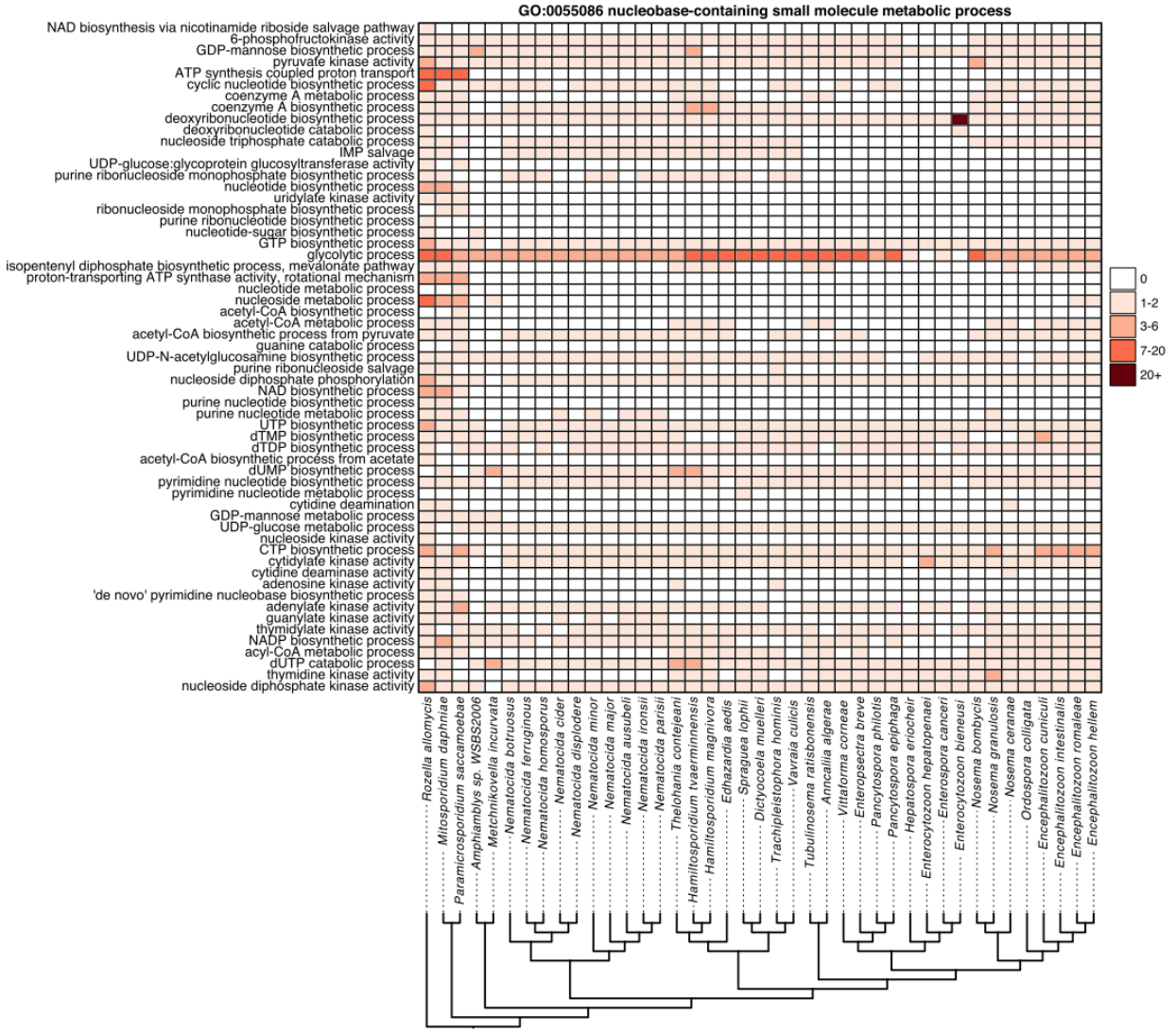

Fig. S11. Conservation of nucleobase-containing small molecule metabolic processes across microsporidia genomes. Membership of proteins from *R. allomycis* and 40 microsporidia species in descendant GO terms from the Pombe GO-slim category "nucleobase-containing small molecule metabolic process" was determined. The number of proteins from each species determined to belong to each Go term is shown as a heatmap with GO-slim categories in rows and microsporidia species in columns. Only descendant GO terms that contain at least one protein from any of these species is shown. Legend for the number of proteins in each cell is shown at the right. Phylogenetic tree, shown at bottom, was constructed using Orthofinder. Several species (*Pseudoloma neurophilia, Dictyocoela roeselum*, *Cucumispora dikerogammari*, and *Nosema apis*) were excluded on the basis of being poorer quality genome assemblies (See Fig. 1).

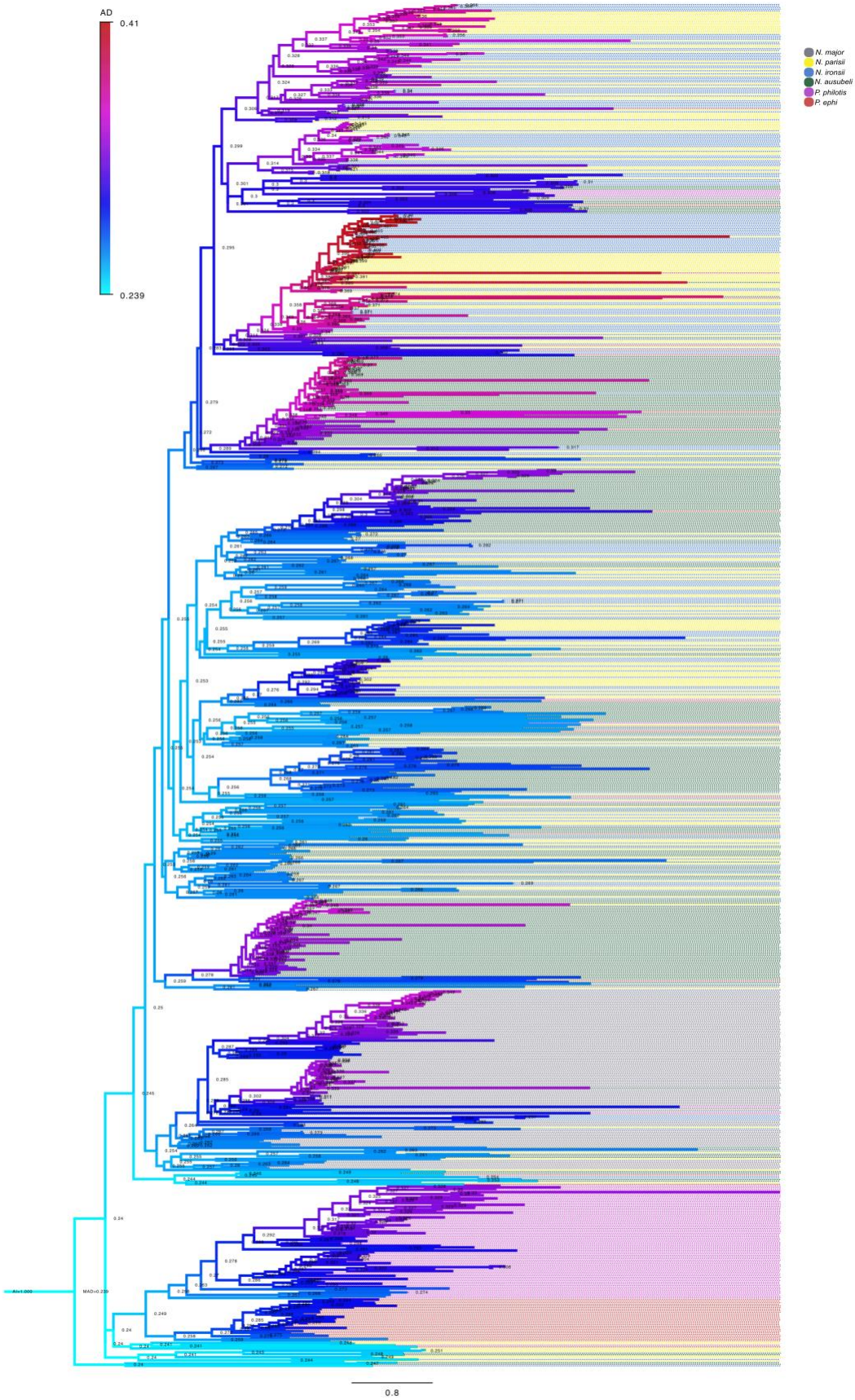
AD
0.41
0.239
N. major
N. parisii
N. ironsii
N. ausubeli
P. philotis
P. ephi
0.8

Fig. S12. Minimal ancestral deviation analysis of NEMLGF1 tree root. Fig. 5. Phylogenetic tree of NemLGF1 family members, colored by species according to the legend at the top right. Each branch is coloured according to ancestral deviation (AD) according to the scale at the top left.

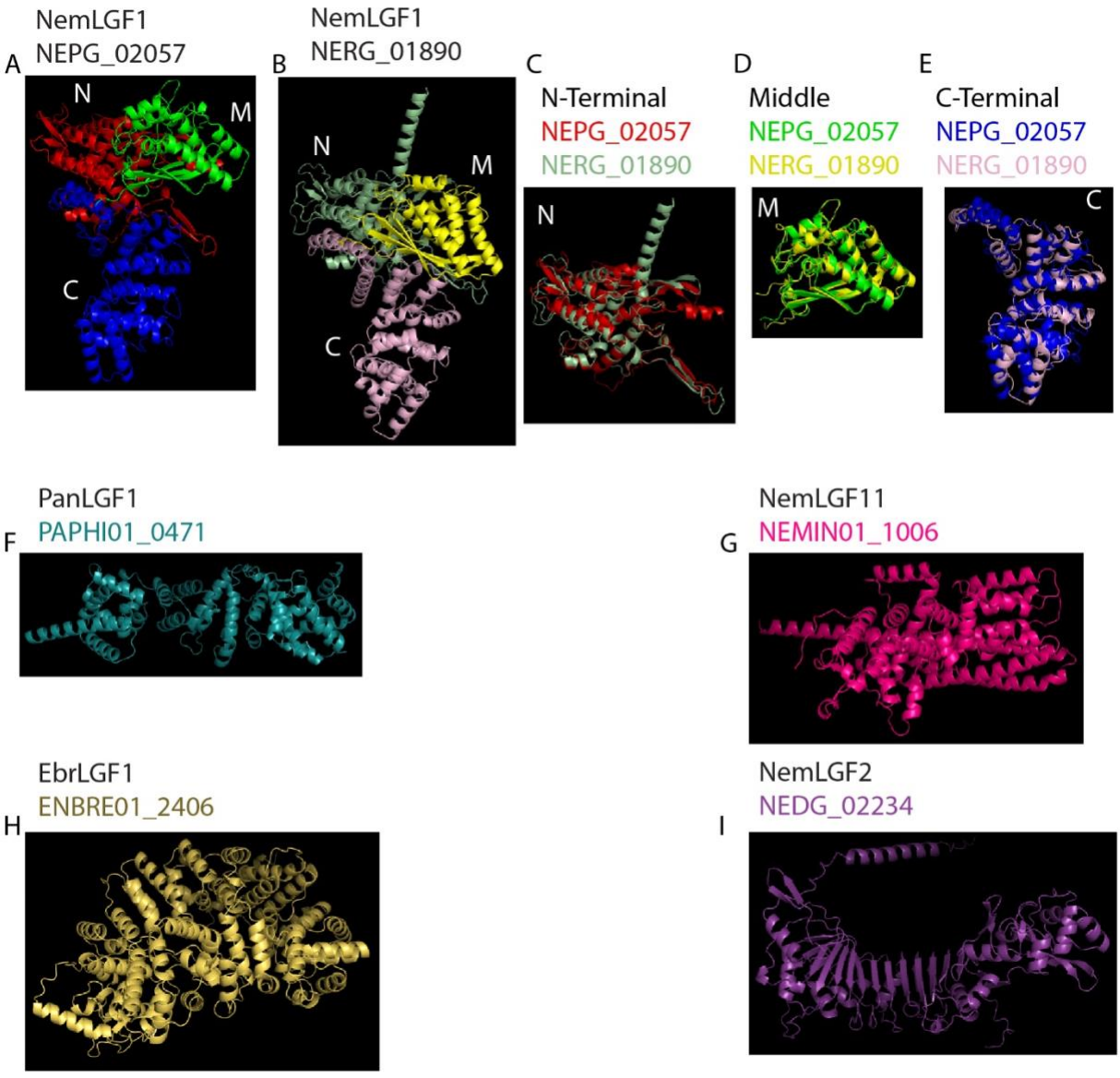

Fig. S13. Structural models of nematode-infecting microsporidia large gene families. Fig. 5. The large gene family NemLGF1 has likely been horizontally transferred between genera. (A-B) AlphaFold models of *N.* parisii NEPG_02057 (B) and *N. ausubeli* NERG_01890

(B). (C-E) Aligned structures of the N-terminal (C), middle (D), and C-terminal (E) domains. N, N-terminal. M, middle. C, C-terminal. (F-I) AlphaFold models of PanLGF1 member PAPHI01_0471 (F), NemLGF11 NEMIN01_1006 (G), EbrLGF1 ENBRE01_2406 (H), and NemLGF2 NEDG_02234 (I).

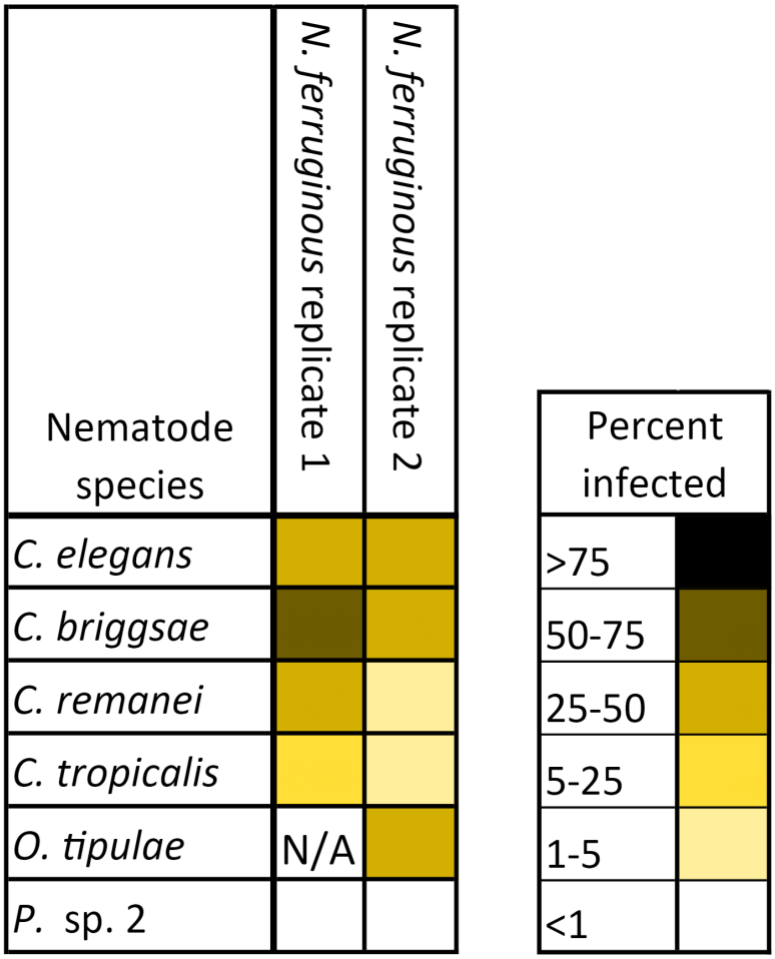

Fig. S14. *N. ferrugionous* infects multiple host species. Six species of L1 stage nematodes were infected with either 20 (replicate 1) or 40 million (replicate 2) *N. ferruginous (*LUAm3) spores. After 96 hours of incubation with spores, animals were fixed and stained with direct yellow 96. Percent of each population of animals infected with each species of microsporidia. Data is displayed as a heat map with host species in rows, each *N. ferruginous* replicate in columns, and the value of each cell being the percent of each population that displayed newly formed microsporidia spores. Legend is displayed at the right. 50-196 animals were counted for each sample.

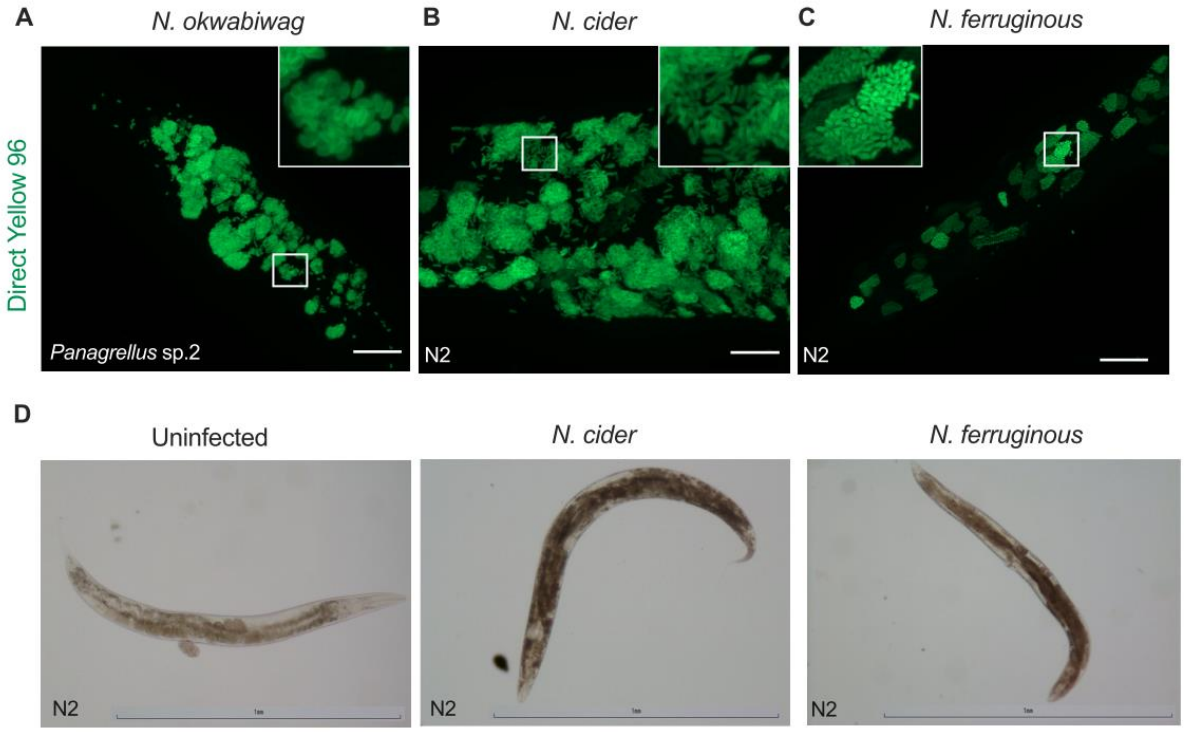

Fig. S15. Spore formation observed in the intestine for *N. botruosus* and throughout the animal for *N. cider* and *N. ferruginous*. (A-C) L1 stage animals were infected for 96 hours, fixed, and stained with DY96. Representative images were taken with the apotome module of a ZEISS Axio Imager at 63x magnification. Multiple z-planes were imaged, and a maximum intensity projection is displayed for each sample. Scale bars, 20 μm. **(A)** *Panagrellus* sp. 2 infected with 28 million *N. botruosus* spores. **(B)** *C. elegans* N2 infected with 4 million *N. cider* spores. **(C)** *C. elegans* N2 infected with 40 million *N. ferruginous* (LUAm3) spores. **(D)** *C. elegans* N2 animals were either infected with 3 million *N. cider* spores or 3 million *N. ferruginous* spores for 5 days. Images taken with Nikon Eclipse Ni at 10 x magnification and displayed.

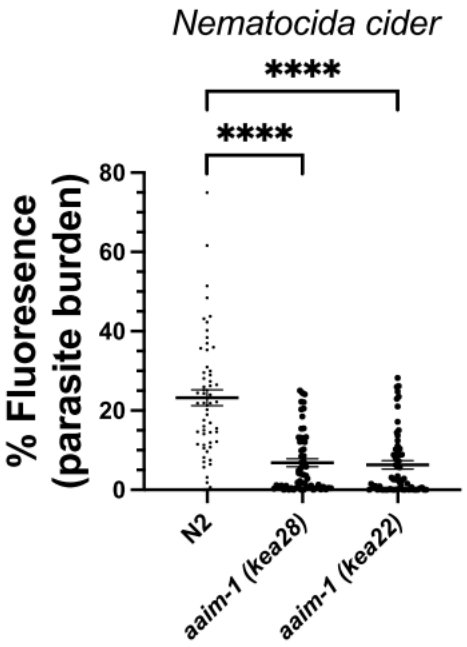

Fig. S16. AAIM-1 is necessary for efficient infection by *N. cider.* N2 and *aaim-1* mutant animals infected with 4 million *N. cider* spores, fixed at 96 hours, and stained with direct-yellow 96 (DY96). 20-30 worms quantified per replicate. % Fluoresence represents percentage of animal carrying DY96 signal, thus reflecting parasite burden, measured via FIJI. Mean ± SEM represented by horizontal bars. P-values determined via One-way Anova with post hoc. Significance defined as **** $p < 0.0001$.

References

1. Vavra, J. & Lukes, J. Microsporidia and 'the art of living together'. *Adv Parasitol* **82**, 253–319 (2013).
2. Katinka, M. D. *et al.* Genome sequence and gene compaction of the eukaryote parasite Encephalitozoon cuniculi. *Nature* **414**, 450–453 (2001).
3. Wadi, L. & Reinke, A. W. Evolution of microsporidia: An extremely successful group of eukaryotic intracellular parasites. *PLoS Pathog* **16**, e1008276 (2020).
4. Capella-Gutiérrez, S., Marcet-Houben, M. & Gabaldón, T. Phylogenomics supports microsporidia as the earliest diverging clade of sequenced fungi. *BMC Biology* **10**, 47 (2012).

5. Cuomo, C. A. *et al.* Microsporidian genome analysis reveals evolutionary strategies for obligate intracellular growth. *Genome Res.* **22**, 2478–2488 (2012).
6. Li, Y. *et al.* A genome-scale phylogeny of the kingdom Fungi. *Current Biology* **31**, 1653-1665.e5 (2021).
7. Quandt, C. A. *et al.* The genome of an intranuclear parasite, Paramicrosporidium saccamoebae, reveals alternative adaptations to obligate intracellular parasitism. *eLife* **6**, e29594 (2017).
8. Haag, K. L. *et al.* Evolution of a morphological novelty occurred before genome compaction in a lineage of extreme parasites. *PNAS* **111**, 15480–15485 (2014).
9. Nakjang, S. *et al.* Reduction and expansion in microsporidian genome evolution: new insights from comparative genomics. *Genome Biol Evol* **5**, 2285–2303 (2013).
10. Barandun, J., Hunziker, M., Vossbrinck, C. R. & Klinge, S. Evolutionary compaction and adaptation visualized by the structure of the dormant microsporidian ribosome. *Nat Microbiol* **4**, 1798–1804 (2019).
11. Desjardins, C. A. *et al.* Contrasting host–pathogen interactions and genome evolution in two generalist and specialist microsporidian pathogens of mosquitoes. *Nature Communications* **6**, 1–12 (2015).
12. Wiredu Boakye, D. *et al.* Decay of the glycolytic pathway and adaptation to intranuclear parasitism within Enterocytozoonidae microsporidia. *Environ Microbiol* **19**, 2077–2089 (2017).
13. Murareanu, B. M. *et al.* Generation of a Microsporidia Species Attribute Database and Analysis of the Extensive Ecological and Phenotypic Diversity of Microsporidia. *mBio* vol. 12 e01490-21 (2021).
14. Luallen, R. J. *et al.* Discovery of a Natural Microsporidian Pathogen with a Broad Tissue Tropism in Caenorhabditis elegans. *PLoS Pathog.* **12**, e1005724 (2016).

15. Zhang, G. *et al.* A Large Collection of Novel Nematode-Infecting Microsporidia and Their Diverse Interactions with Caenorhabditis elegans and Other Related Nematodes. *PLoS Pathog* **12**, e1006093 (2016).
16. Troemel, E. R., Felix, M.-A., Whiteman, N. K., Barriere, A. & Ausubel, F. M. Microsporidia are natural intracellular parasites of the nematode Caenorhabditis elegans. *PLoS Biol* **6**, 2736–2752 (2008).
17. Reinke, A. W., Balla, K. M., Bennett, E. J. & Troemel, E. R. Identification of microsporidia host-exposed proteins reveals a repertoire of rapidly evolving proteins. *Nat Commun* **8**, 14023 (2017).
18. Willis, A. R. *et al.* A parental transcriptional response to microsporidia infection induces inherited immunity in offspring. *Science Advances* **7**, eabf3114 (2021).
19. Tamim El Jarkass, H. *et al.* An intestinally secreted host factor promotes microsporidia invasion of C. elegans. *eLife* **11**, e72458 (2022).
20. Bakowski, M. A. *et al.* Ubiquitin-mediated response to microsporidia and virus infection in C. elegans. *PLoS Pathog* **10**, e1004200 (2014).
21. Szumowski, S. C., Botts, M. R., Popovich, J. J., Smelkinson, M. G. & Troemel, E. R. The small GTPase RAB-11 directs polarized exocytosis of the intracellular pathogen N. parisii for fecal-oral transmission from C. elegans. *Proc Natl Acad Sci U S A* **111**, 8215–8220 (2014).
22. Murareanu, B. M., Knox, J., Roy, P. J. & Reinke, A. W. High-throughput small molecule screen identifies inhibitors of microsporidia invasion and proliferation in C. elegans. *bioRxiv* 2021.09.06.459184 (2021) doi:10.1101/2021.09.06.459184.
23. Tecle, E. & Troemel, E. R. Insights from C. elegans into Microsporidia Biology and Host-Pathogen Relationships. *Exp Suppl* **114**, 115–136 (2022).
24. Emms, D. M. & Kelly, S. OrthoFinder: phylogenetic orthology inference for comparative genomics. *Genome Biology* **20**, 238 (2019).

25. Vossbrinck, C. R. & Debrunner-Vossbrinck, B. A. Molecular phylogeny of the Microsporidia: ecological, ultrastructural and taxonomic considerations. *Folia Parasitologica* **52**, 131–142 (2013).
26. Bojko, J. *et al.* Microsporidia: a new taxonomic, evolutionary, and ecological synthesis. *Trends in Parasitology* **0**, (2022).
27. Stentiford, G. D., Bass, D. & Williams, B. A. P. Ultimate opportunists—The emergent Enterocytozoon group Microsporidia. *PLOS Pathogens* **15**, e1007668 (2019).
28. Huang, Q. Evolution of Dicer and Argonaute orthologs in microsporidian parasites. *Infection, Genetics and Evolution* **65**, 329–332 (2018).
29. Dia, N. *et al.* InterB multigenic family, a gene repertoire associated with subterminal chromosome regions of Encephalitozoon cuniculi and conserved in several human-infecting microsporidian species. *Curr Genet* **51**, 171–186 (2007).
30. Tria, F. D. K., Landan, G. & Dagan, T. Phylogenetic rooting using minimal ancestor deviation. *Nat Ecol Evol* **1**, 1–7 (2017).
31. Highly accurate protein structure prediction with AlphaFold | Nature. https://www.nature.com/articles/s41586-021-03819-2.
32. ColabFold: making protein folding accessible to all | Nature Methods. https://www.nature.com/articles/s41592-022-01488-1.
33. Willis, A. R. & Reinke, A. W. Factors That Determine Microsporidia Infection and Host Specificity. *Exp Suppl* **114**, 91–114 (2022).
34. Luallen, R. Infection strategies of related Nematocida microsporidian species in their natural host, Caenorhabditis elegans. (UC San Diego, 2016).
35. Han, B. & Weiss, L. M. Microsporidia: Obligate Intracellular Pathogens within the Fungal Kingdom. *Microbiol Spectr* **5**, (2017).

36. Weidner, E., Manale, S. B., Halonen, S. K. & Lynn, J. W. Protein-Membrane Interaction Is Essential to Normal Assembly of the Microsporidian Spore Invasion Tube. *Biol Bull* **188**, 128–135 (1995).
37. Julian, A. T., Mascarenhas dos Santos, A. C. & Pombert, J.-F. 3DFI: a pipeline to infer protein function using structural homology. *Bioinformatics Advances* **1**, vbab030 (2021).
38. Mascarenhas dos Santos, A. C., Julian, A. T. & Pombert, J.-F. The Rad9–Rad1–Hus1 DNA Repair Clamp is Found in Microsporidia. *Genome Biology and Evolution* **14**, evac053 (2022).
39. Trzebny, A., Slodkowicz-Kowalska, A., Becnel, J. J., Sanscrainte, N. & Dabert, M. A new method of metabarcoding Microsporidia and their hosts reveals high levels of microsporidian infections in mosquitoes (Culicidae). *Molecular Ecology Resources* **20**, 1486–1504 (2020).
40. Reinke, A. W. & Troemel, E. R. The Development of Genetic Modification Techniques in Intracellular Parasites and Potential Applications to Microsporidia. *PLoS Pathog* **11**, e1005283 (2015).
41. Huang, Y. *et al.* A secretory hexokinase plays an active role in the proliferation of Nosema bombycis. *PeerJ* **6**, e5658 (2018).
42. Paldi, N. *et al.* Effective Gene Silencing in a Microsporidian Parasite Associated with Honeybee (*Apis mellifera*) Colony Declines. *Applied and Environmental Microbiology* vol. 76 5960–5964 (2010).
43. Saleh, M. *et al.* In Vitro Gene Silencing of the Fish Microsporidian Heterosporis saurida by RNA Interference. *Nucleic Acid Therapeutics* **26**, 250–256 (2016).
44. Kim, I.-H., Kim, D.-J., Gwak, W.-S. & Woo, S.-D. Increased survival of the honey bee Apis mellifera infected with the microsporidian Nosema ceranae by effective gene silencing. *Archives of Insect Biochemistry and Physiology* **105**, e21734 (2020).
45. Zheng, S. *et al.* The role of NbTMP1, a surface protein of sporoplasm, in Nosema bombycis infection. *Parasites & Vectors* **14**, 81 (2021).

46. Chen, L., Li, R., You, Y., Zhang, K. & Zhang, L. A Novel Spore Wall Protein from Antonospora locustae (Microsporidia: Nosematidae) Contributes to Sporulation. *Journal of Eukaryotic Microbiology* **64**, 779–791 (2017).

47. Kamath, R. S. & Ahringer, J. Genome-wide RNAi screening in Caenorhabditis elegans. *Methods* **30**, 313–321 (2003).

48. Barriere, A. & Felix, M.-A. Isolation of C. elegans and related nematodes. *WormBook* 1–19 (2014) doi:10.1895/wormbook.1.115.2.

49. Martin, M. Cutadapt removes adapter sequences from high-throughput sequencing reads. *EMBnet.journal* vol. 17 3 (2011).

50. Bolger, A. M., Lohse, M. & Usadel, B. Trimmomatic: a flexible trimmer for Illumina sequence data. *Bioinformatics* **30**, 2114–2120 (2014).

51. Langmead, B. & Salzberg, S. L. Fast gapped-read alignment with Bowtie 2. *Nat Methods* **9**, 357–359 (2012).

52. Simpson, J. T. *et al.* ABySS: A parallel assembler for short read sequence data. *Genome Res.* **19**, 1117–1123 (2009).

53. Laetsch, D. R. & Blaxter, M. L. BlobTools: Interrogation of genome assemblies. Preprint at https://doi.org/10.12688/f1000research.12232.1 (2017).

54. Pryszcz, L. P. & Gabaldón, T. Redundans: an assembly pipeline for highly heterozygous genomes. *Nucleic Acids Research* **44**, e113 (2016).

55. Johnson, M. *et al.* NCBI BLAST: a better web interface. *Nucleic Acids Res* **36**, W5–W9 (2008).

56. Hyatt, D. *et al.* Prodigal: prokaryotic gene recognition and translation initiation site identification. *BMC Bioinformatics* **11**, 119 (2010).

57. Eddy, S. R. Accelerated Profile HMM Searches. *PLOS Computational Biology* **7**, e1002195 (2011).

58. Finn, R. D. *et al.* The Pfam protein families database: towards a more sustainable future. *Nucleic Acids Res* **44**, D279-285 (2016).

59. Petersen, T. N., Brunak, S., von Heijne, G. & Nielsen, H. SignalP 4.0: discriminating signal peptides from transmembrane regions. *Nat Methods* **8**, 785–786 (2011).

60. Krogh, A., Larsson, B., von Heijne, G. & Sonnhammer, E. L. L. Predicting transmembrane protein topology with a hidden markov model: application to complete genomes11Edited by F. Cohen. *Journal of Molecular Biology* **305**, 567–580 (2001).

61. Mi, H., Muruganujan, A., Casagrande, J. T. & Thomas, P. D. Large-scale gene function analysis with the PANTHER classification system. *Nat Protoc* **8**, 1551–1566 (2013).

62. Mitchell, A. L. *et al.* InterPro in 2019: improving coverage, classification and access to protein sequence annotations. *Nucleic Acids Research* **47**, D351–D360 (2019).

63. James, T. Y. *et al.* Shared Signatures of Parasitism and Phylogenomics Unite Cryptomycota and Microsporidia. *Current Biology* **23**, 1548–1553 (2013).

64. Simão, F. A., Waterhouse, R. M., Ioannidis, P., Kriventseva, E. V. & Zdobnov, E. M. BUSCO: assessing genome assembly and annotation completeness with single-copy orthologs. *Bioinformatics* **31**, 3210–3212 (2015).

65. Li, L., Stoeckert, C. J. J. & Roos, D. S. OrthoMCL: identification of ortholog groups for eukaryotic genomes. *Genome Res* **13**, 2178–2189 (2003).

66. HHblits: lightning-fast iterative protein sequence searching by HMM-HMM alignment | Nature Methods. https://www.nature.com/articles/nmeth.1818.

67. Using Dali for Protein Structure Comparison - PubMed. https://pubmed.ncbi.nlm.nih.gov/32006276/.

68. Schindelin, J. *et al.* Fiji: an open-source platform for biological-image analysis. *Nature Methods* **9**, 676–682 (2012).

69. Schneider, C. A., Rasband, W. S. & Eliceiri, K. W. NIH Image to ImageJ: 25 years of image analysis. *Nat Methods* **9**, 671–675 (2012).